iScience

CellPress
OPEN ACCESS

Article

# Dental pulp stem cells promote genioglossus repair and systemic amelioration in chronic intermittent hypoxia

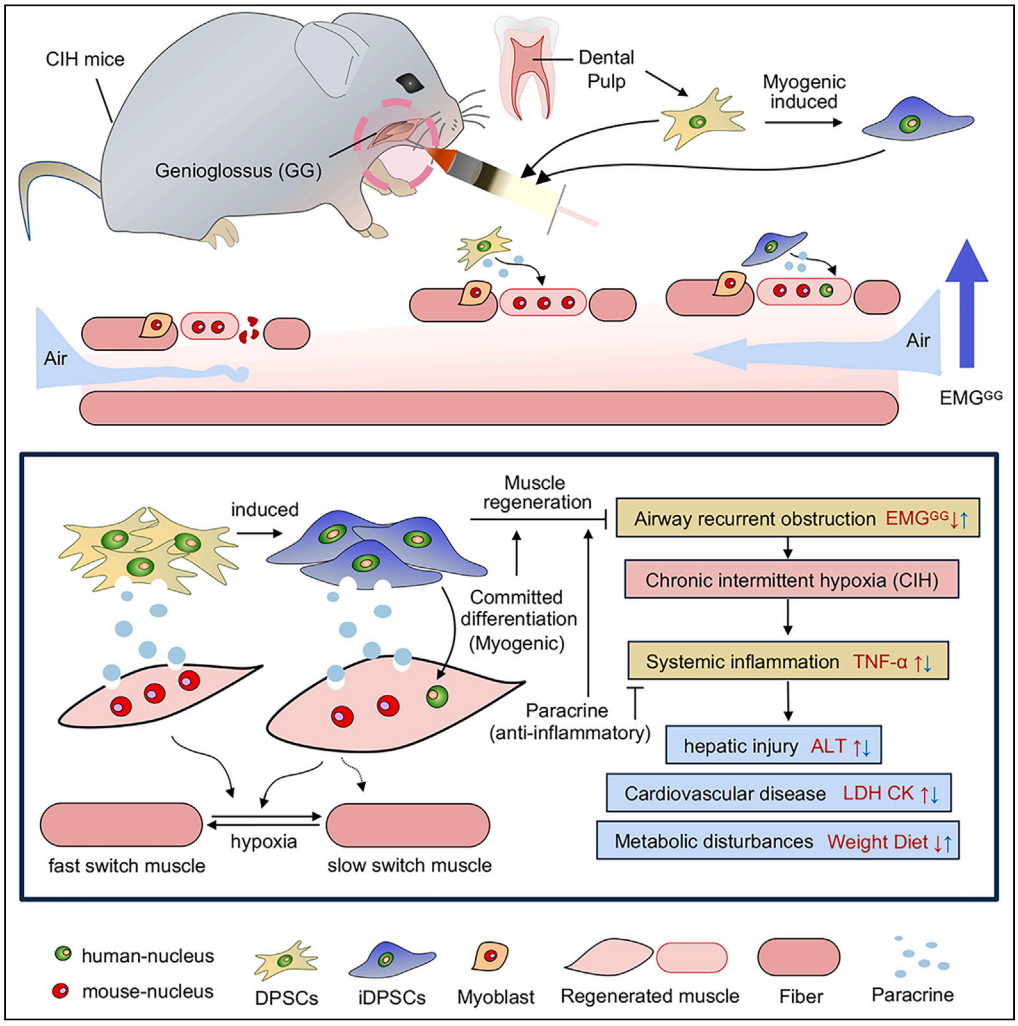


Meng-Han Zhang, Wei-Hua Zhang, Yun Lu, ..., Meng-Jie Wu, Wang-Hui Ding, Yue-Hua Liu

godson888@zju.edu.cn (W.-H.D.)
liuyuehua@fudan.edu.cn (Y.-H.L.)

## Highlights

DPSCs/iDPSCs improve $EMG^{GG}$, muscle fiber type transition, systemic inflammation in CIH mice

iDPSCs enhance GG repair in CIH mice by elevating expression of MyoD and Pax7 vs. DPSCs

Both DPSCs and iDPSCs promote muscle regeneration via paracrine effects

iDPSCs directly aid myogenic differentiation, seen human-derived myogenic transcripts

Zhang et al., iScience 27, 111143
November 15, 2024 
https://doi.org/10.1016/j.isci.2024.111143

iScience

CellPress
OPEN ACCESS

Article

# Dental pulp stem cells promote genioglossus repair and systemic amelioration in chronic intermittent hypoxia

Meng-Han Zhang,[1,2,3] Wei-Hua Zhang,[2,3] Yun Lu,[2] Li-Ming Yu,[2] Xin-Xin Han,[2] Yan Xu,[2] Meng-Jie Wu,[1] Wang-Hui Ding,[1,*] and Yue-Hua Liu[2,4,*]

## SUMMARY

**Obstructive sleep apnea (OSA) leads to chronic intermittent hypoxia (CIH) and is not well addressed by current therapies. The genioglossus (GG) is the largest upper airway dilator controlling OSA pathology, making its repair a potential treatment. This study investigates dental pulp stem cells (DPSCs) in repairing GG injury in a CIH mouse model. We induced DPSCs to myogenic lineage cells (iDPSCs) and transplanted them into GG of CIH mice. DPSCs/iDPSCs grafts improved $EMG^{GG}$ and muscle type transitions while reducing tumor necrosis factor α (TNF-α), alanine aminotransferase (ALT), lactate dehydrogenase (LDH), and creatine kinase (CK) levels, improving body weight. Moreover, iDPSCs increased $Pax7^{+}$/$Ki67^{+}$ and human-derived STEM121 cells in the GG compared with DPSCs. DPSCs/iDPSCs enhanced $Desmin^{+}$ myotube formation in myoblasts under hypoxia *in vitro*, with iDPSCs increased human-derived myogenic markers and nuclei in myotubes. These results indicate that iDPSCs, beyond their paracrine effects like DPSCs, directly participate in myogenic differentiation, supporting the potential use of DPSCs for OSA treatment.**

## INTRODUCTION

Obstructive sleep apnea (OSA) is a common disorder characterized by recurrent episodes of upper airway collapse during sleep. There is increasing evidence that anatomical stenosis of the upper airway does not invariably result in OSA.[1] The function of upper respiratory dilators is crucial for maintaining upper airway patency during sleep.[2] The activity of upper airway dilators in OSA patients decreased at sleep, making them unable to compensate for anatomical deficiencies, which leads to airway obstruction.[3] In this case, carbon dioxide levels, negative pressure, and respiratory drive continue to increase until waking up from sleep, at which point the airway reopened.[4] This recurrent airway obstruction can lead to the development of chronic intermittent hypoxia (CIH), making the pharyngeal dilator more susceptible to fatigue. CIH, a hallmark manifestation of OSA, triggers sympathetic activation, leading to spikes in blood pressure and cardiac workload, elevating inflammatory products and reactive oxygen species, and ultimately causing systemic inflammation.[5] Increased cardiac workload and the resulting inflammation can lead to metabolic disturbances and endothelial dysfunction, consequently, cardiovascular disease.[6,7] OSA/CIH is also associated with increased liver fibrosis, oxidative damage, and hepatic inflammatory injury.[8] All in all, OSA may eventually lead to a series of complications and even sudden death.[9]

The genioglossus (GG) is the largest dilator muscle controlling the upper airway. The onset of apnea is strongly correlated with a decline in GG activity during sleep, but this is not well addressed by current therapy.[10] Continuous positive airway pressure (CPAP), surgery, or oral appliances can only mechanically expand the upper airway, with limited capacity to improve GG function.[11] Although hypoglossal nerve stimulation is dedicated to GG function, it stimulates the nerve through invasively implanted devices to induce GG contraction rather than to protect the GG itself, with varying response and unknown long-term effects.[12] Therefore, a promising therapeutic approach is urged to protect GG and effectively improve GG function.

Dental pulp stem cells (DPSCs) are mesenchymal stem cells (MSCs) derived from dental pulp that have wide implications in regenerative medicine due to several advantages: better proliferative and multi-differentiation potential, a simpler primary isolation method, long-term storage capability, immunomodulatory properties, and low immunogenicity.[13–16] Evidence shows that DPSCs can be myogenically

[1]Stomatology Hospital, School of Stomatology, Zhejiang University School of Medicine, Zhejiang Provincial Clinical Research Center for Oral Diseases, Key Laboratory of Oral Biomedical Research of Zhejiang Province, Cancer Center of Zhejiang University, Engineering Research Center of Oral Biomaterials and Devices of Zhejiang Province, Hangzhou 310000, China
[2]Shanghai Key Laboratory of Craniomaxillofacial Development and Diseases, Shanghai Stomatological Hospital & School of Stomatology, Fudan University, Shanghai 200001, China
[3]These authors contributed equally
[4]Lead contact
*Correspondence: godson888@zju.edu.cn (W.-H.D.), liuyuehua@fudan.edu.cn (Y.-H.L.)
https://doi.org/10.1016/j.isci.2024.111143

induced[17,18] and have therapeutic potential for muscle injury.[19] At present, DPSCs transplantation can indeed repair muscle injury by secreting multiple factors with no immune rejection[16] but not by direct contribution to myogenic differentiation. Compared to other muscle-derived cells, the efficiency of MSCs in muscle formation is relatively low.[20] Studies have shown that myogenic-induced MSCs may increase transplantation efficiency.[21] However, it remains unclear whether myogenic induction of DPSCs can enhance the transplantation efficiency, and its repair effect on GG muscle in OSA/CIH has not been fully studied.

In our study, DPSCs were myogenic induced (iDPSCs). We then implanted DPSCs/iDPSCs into the GG of CIH mice to test their potential treatment for OSA. We explored the possibility of DPSCs as a cell source of cells for OSA treatment.

## RESULTS

### DPSCs/iDPSCs transplantation relieved muscle hypertrophy and improved electromyography of GG in CIH mice

To investigate the impact of DPSCs/iDPSCs on GG in OSA, we examined the structure and function of GG in CIH mice after DPSCs/iDPSCs transplantation. Firstly, DPSCs were myogenic induced to iDPSCs showing high expression of muscle stem cell marker Pax7 (Figure 1A) and these iDPSCs can be differentiated into multinuclear myotube-like cells (Figure 1B). Then we established CIH modeling to imitate OSA by placing mice in chambers controlled by a computerized delivery profile system connected to $N_2$ and $O_2$ (Figure 1C), regulating 21%–7.5% $O_2$ circulation (Figure 1D). DPSCs/iDPSCs were transplanted into the GG of mice (Figure 1E), and the injection position was proved by anatomy (left) and histology (right) pre-experiment (Figure 1F). DPSCs/iDPSCs was injected at the fourth-week of CIH exposure, structure and function examinations were tested at the sixth-week of CIH exposure (Figure 1G).

We found the structural changes in GG using H&E and Masson staining (Figure 2A). CIH showed a mild muscle fiber hypertrophy (Figure 2B), and iDPSCs reduced the proportion of larger muscle bundles with a 1,300 $\mu m^2$ area, thus relieving muscle hypertrophy (Figure 2C). To determine the effect of stem cell therapy on GG function, electromyography of the GG ($EMG^{GG}$) was performed (Figures 2D and 2E). Both DPSCs and iDPSCs treatments significantly increased the mean and max frequencies, as well as the mean amplitude of $EMG^{GG}$ (Figures 2F–2H). Notably, iDPSCs also increased the max amplitude and min frequency of $EMG^{GG}$ (Figures 2I and 2J), yet there was no statistically significant improvement in min amplitude (Figure 2K). It implied that both DPSCs and iDPSCs can improve GG function of CIH mice, with iDPSCs showing better performance. Notably, a mild T cell infiltration with activated FasL/PDL1 was observed after DPSCs/iDPSCs injection in GG, but it is relatively rare, verifying their low immunogenicity (Figure S1).

In addition, GG works in conjunction with other muscle groups, such as the geniohyoid, mylohyoid, and digastric muscles (DM), to control the position of the tongue, hyoid, jaw, and chin, which play an important role in OSA pathology.[22] Due to the small volume of the GG, local stem cell injection may affect adjacent tissues, such as DM. Therefore, the EMG signals of DM ($EMG^{DM}$) were also detected. No significant differences were found among the measurement indicators after DPSCs/iDPSCs treatment, except for a slight improvement in mean frequency (Figure S2). This may indicate the relative accuracy of the injection.

### DPSCs/iDPSCs transplantation reduced the ratio of fast to slow twitch muscle fibers in CIH mice

The diverse distribution patterns of muscle fiber types are the physiological basis for muscle function differences. Myosin heavy chain (MyHC) protein is the molecular marker used to distinguish muscle fiber types, with the isomers of MyHC-I (MYH7b) and the isomers of MyHC-IIA (MYH2), MyHC-IIB (MYH4), and MyHC-IIX (MYH1) corresponding to the slow-twitch (aerobic) and fast-twitch (anaerobic) muscle fibers, respectively (Figure 3A).[23] Upper airway dilator muscles undergo a slow to fast fiber-type transition in OSA/CIH models. To explore the histological basis of DPSC/iDPSC grafts on GG function, the distribution of fiber types in the GG was evaluated. Firstly, we tested the relative mRNA expression of MYH2 (Figure 3B), MYH4 (Figure 3C), MYH1 (Figure 3D), and MYH7b (Figure 3E) in GG. Both DPSCs and iDPSCs treatments can reduce the mRNA expression levels of fast-twitch genes MYH1, MYH2, and MYH4 (Figures 3C–3E) yet with no significant difference in the expression of slow-twitch gene MYH7b among the groups (Figure 3B). Secondly, we measured the protein levels of MyHC-I (Figure 3F), MyHC-IIA (Figure 3G), MyHC-IIB (Figure 3H), and MyHC-IIX (Figure 3I) in GG using immunofluorescence. Both DPSCs and iDPSCs treatments can increase the levels of slow-twitch protein MyHC-I (Figure 3J). However, only iDPSCs can reduce the levels of fast-twitch proteins MyHC-IIA and MyHC-IIB in GG tissue (Figures 3K and 3L) with no improvement on MyHC-IIX (Figure 3M). It is implied that both DPSCs and iDPSCs can encourage a more aerobic fiber type from fast to slow in GG of CIH mice, with iDPSCs showing better performance. To further validate the increased aerobic respiration, mitochondrial activity levels were measured by immunohistochemistry of succinate dehydrogenase (SDHA) in GG of CIH mice (Figure 3N). The results showed that iDPSCs can significantly increase the SDHA levels in the GG of CIH mice (Figure 3O), implying enhanced aerobic respiration after iDPSCs treatment.

To further explore the systemic action of DPSC/iDPSC grafts, the distribution of fiber types in the lower limb gastrocnemius muscle (GA) was also evaluated. We found that both DPSCs and iDPSCs treatments can reduce the mRNA expression levels of the slow-twitch gene MYH7b (Figure 4A) and increase the fast-twitch genes MYH1, MYH2, and MYH4 (Figures 4B–4D) in the GA of CIH mice. We then measured the protein levels of MyHC-I, MyHC-IIA (Figure 4E), MyHC-IIB, and MyHC-IIX (Figure 4F) in GA using immunofluorescence. Both DPSCs and iDPSCs treatments can increase the levels of slow-twitch protein MyHC-I (Figure 4G). However, only iDPSCs can also reduce the levels of fast-twitch protein MyHC-IIA in GG tissue (Figure 4H) with no improvement on MyHC-IIB and MyHC-IIX (Figures 4I and 4J). Next, to better quantify the aerobic respiration for fueling slow-twitch muscle fibers, mitochondrial activity levels were also assessed in GA using SDHA staining (Figure 4K). Regarding the hypoxia adaptation in fatigue-resistant muscles of the lower limb muscles (e.g., GA) are not as sensitive as those in the upper airway muscles (e.g., GG) in OSA/CIH state, the baseline for aerobic respiration was not high in GA.[24] The results revealed that the abundance of SDHA was relatively low in GA (Figure 4K). However, iDPSCs therapy can still increase the levels of SDHA in GA (Figure 4L),

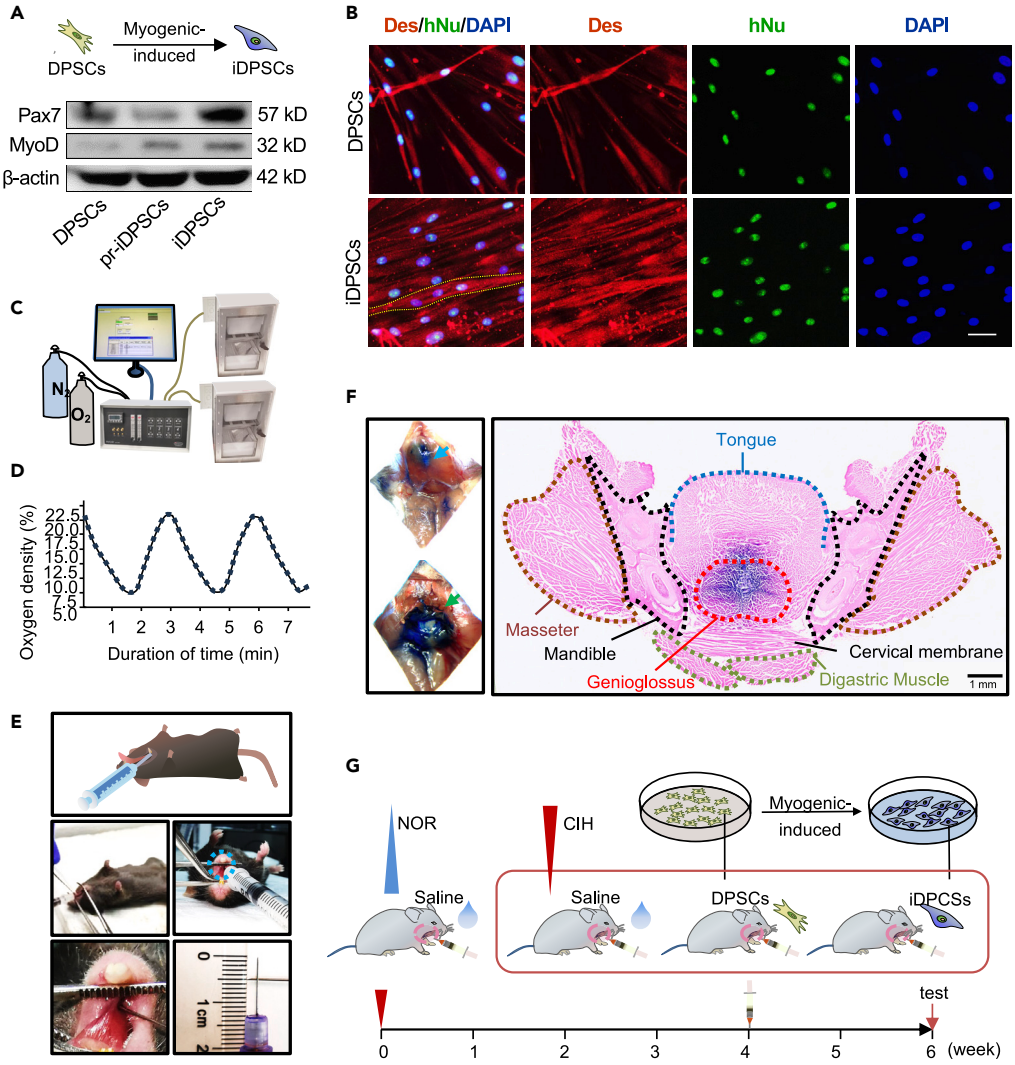


**Figure 1. DPSCs/iDPSCs were transplanted into the GG of CIH mice**

(A) Protein expression of Pax7 and MyoD were assessed using western blot after DPSCs were myogenic-induced to pr-iDPSCs with 5-Aza and finally to iDPSCs following with BMP antagonists.

(B) Immunofluorescence staining with Desmin (red), hNu (green), and DAPI (blue) after DPSCs/iDPSCs were myogenic differentiated. Yellow dotted line indicated the outline of myotube-like cell. Scale, 40 μm. Des: Desmin. hNu: human nuclei.

(C) Establishment of CIH animal model.

(D) A schematic diagram reporting 21%–7.5% O2 180s a circle.

(E) Schematic diagram of GG injection operation from lateral and frontal view, showing injection position and depth.

(F) The correction of injection position was verified by crystal violet solution injected into GG. Anatomy proof of injection position (left): blue arrow indicates DM. Green arrow indicates GG muscle. Histological proof of injection position was displaced by position of masseter, mandible, cervical membrane, tongue, digastric muscle, and purple-stained GG in cross section of head and neck. Scale, 1 mm.

(G) Animals were divided into four groups: NOR, CIH, CIH + DPSCs, and CIH + iDPSCs. CIH was exposed for six months, and DPSCs/iDPSCs or control saline were transplanted into the GG of mice at the end of 4th week.

promoting a transition to a more aerobic fiber type from fast to slow in the GA of CIH mice. It is implied that DPSC/iDPSC grafts can have a systemic effect, inducing a transition from fast to slow fiber types in limb muscles in CIH mice.

## DPSCs/iDPSCs transplantation reduces TNF-α, ALT, LDH, and CK levels in CIH mice

OSA is linked to the onset of various systemic complications. CIH caused by recurrent airway obstruction would induce sympathetic activation, oxidative stress, and systemic inflammation (elevated tumor necrosis factor α [TNF-α] and C-reactive protein [CRP]), consequently, developing

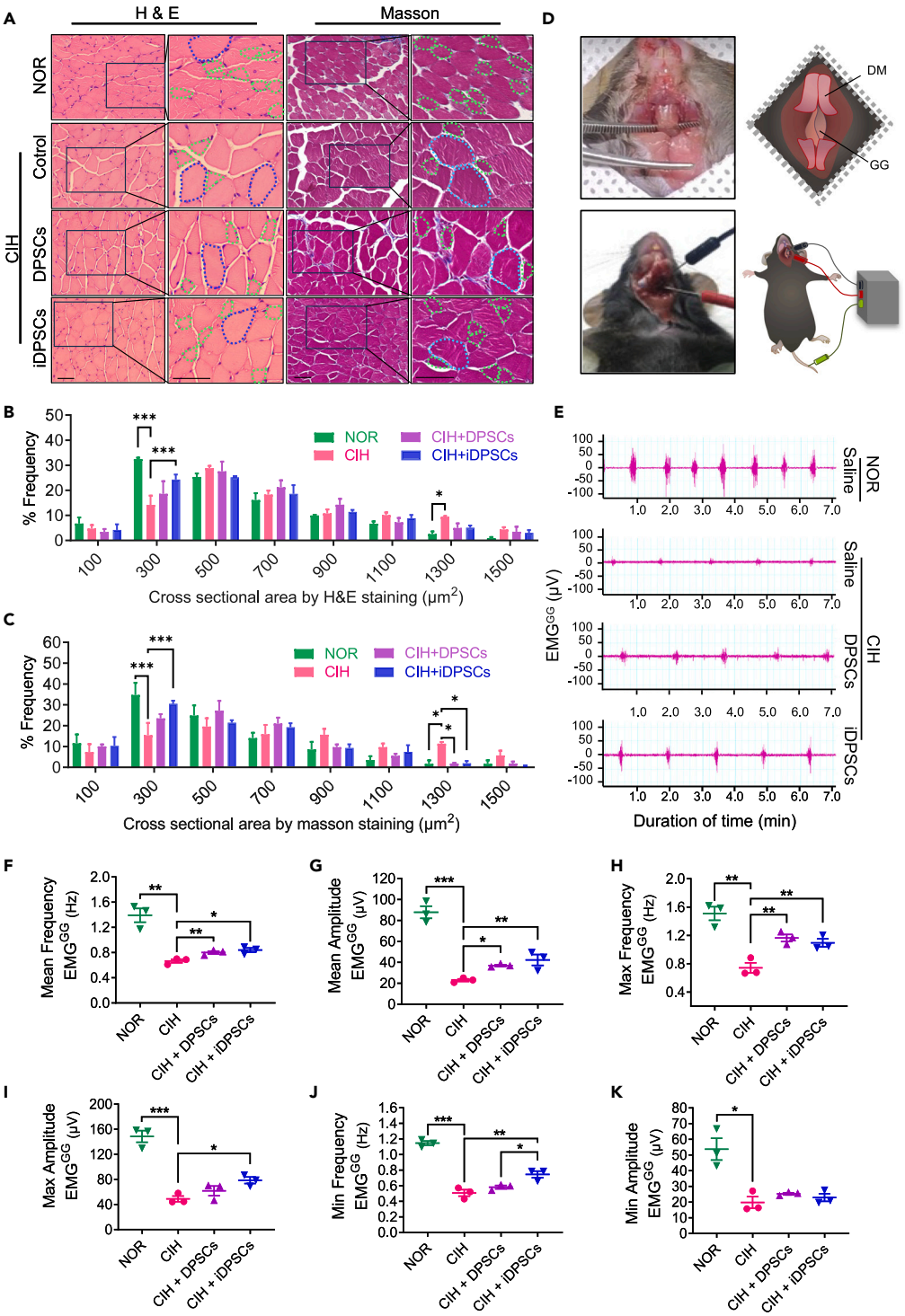


**Figure 2. DPSCs transplantation improved the EMG$^{GG}$ in CIH mice**

(A–C) H&E and Masson staining of GG (A), and cross sectional area of muscle bundle were analyzed by ordered categorical variables for H&E (B) and Masson staining (C), respectively. 300 μm$^2$ represents muscle bundles with an area range of 200–400 μm2, and so on. Green dots indicate ≈300 μm$^2$ muscle bundle, Blue dots indicate ≈1,300 μm$^2$ muscle bundle. Scale, 50 μm. Data are shown as mean ± SEM, $n = 3$, two-way ANOVA by Fisher's LSD test for multiple comparison, $^*p < 0.05$, $^{**}p < 0.01$, $^{***}p < 0.001$.

(D) Schematic diagrams of EMG$^{GG}$ detection: GG were exposed after stripping DM with cervical fascia, and the electrodes were inserted to record EMG$^{GG}$.

**Figure 2. *Continued***

(E–K) EMG signals of GG were detected (E), and quantitative analysis was conducted including mean frequency (F), mean amplitude (G), max frequency (H), max amplitude (I), min frequency (J) and min amplitude (K). CIH, chronic intermittent hypoxia; NOR, normoxia; DPSCs, dental pulp stem cells; iDPSCs, myogenic induced DPSCs; GG, genioglossus; DM, digastric muscles; $EMG^{GG}$, electromyogram of GG; max, maximum; min, minimum. Data are shown as mean ± SEM, $n = 3$, Student's t test for NOR vs. CIH, One-way ANOVA for CIH vs. CIH + DPSCs vs. CIH + iDPSCs by Fisher's LSD test for multiple comparison, $^{*}p < 0.05$, $^{**}p < 0.01$, $^{***}p < 0.001$.

to cardiovascular disease (elevated lactate dehydrogenate [LDH] and creatine kinase [CK]), hepatic injury (elevated aspartate aminotransferase [AST] and alanine aminotransferase [ALT]) and kidney disease (elevated Cre), etc (Figure 5A).[6,25] To test DPSCs/iDSPCs therapy on the development of OSA complications, the serum levels of ALT, AST, CK, Cre, and LDH, as well as the plasma levels of TNF-α and CRP, were measured after DPSCs/iDSPCs therapy. In our study, CIH increased the levels of TNF-α (Figure 5B), CRP (Figure 5C), ALT (Figure 5D), AST (Figure 5E), LDH (Figure 5F), and Cre (Figure 5G) in mice compared with the normoxia (NOR) group. Both DPSC and iDPSC treatments significantly reduced the levels of TNF-α (Figure 5B), ALT (Figure 5D), LDH (Figure 5F), and CK (Figure 5H) and but not CRP (Figure 5C), AST (Figure 5E), and Cre (Figure 5G) levels in CIH mice. This implies that DPSCs/iDSPCs therapy can reduce systemic inflammation factors, thereby improving cardiac and liver function.

## DPSCs/iDPSCs transplantation improved body weight, food intake, and water consumption in CIH mice

To investigate the effect of DPSCs/iDSPCs therapy on diet and weight, food intake, water consumption, and body weight were measured in CIH mice after DPSCs/iDPSCs treatments. In our study, we found that CIH restrained body weight gain in mice compared to the NOR group. When stem cells (or control saline) were transplanted at the end of the $4^{th}$ week, the body weights were temporarily reduced in CIH exposure but were not significantly affected in NOR. By the end of the $5^{th}$ week, stem cell therapy led to weight gain. By the end of the $6^{th}$ week, the temporary weight loss caused by the injection process had ceased. The body weights of mice in both DPSCs and iDPSCs groups were significantly higher than those in CIH groups, and iDPSC groups exhibited greater weight gain than the DPSC groups (Figure 5I).

Similarly, the mean food intake and water consumption of mice decreased after 4 weeks of CIH. When stem cells (or control saline) were injected at the 4th week, the water consumption of all groups decreased temporarily, and the food intake of the hypoxia groups also decreased. By the 5th week, the mean food intake significantly increased under iDPSCs treatment (Figure 5J). By the 6th week, the temporary changes induced by the injection had almost ceased. The mean water consumption and food intake of both DPSCs and iDPSCs groups were much higher than those of the CIH alone group (Figures 5J and 5K). We speculated that DPSCs/iDPSCs therapy may improve weight gain by controlling diet.

## DPSCs/iDPSCs promote myogenic repair of GG in CIH mice, with iDPSCs directly participate to muscle regeneration

Given that muscle regeneration requires activated satellite cells ($Pax7^{+}$) to differentiate into myoblasts ($MyoD^{+}$) for muscle repair, while another subset achieve self-renewal (Figure 6A). To test the myogenic repair of DPSCs/iDPSCs, the expression levels of Pax7 and MyoD in GG were measured. Firstly, the mRNA expressions of Pax7 and MyoD in the GG after DPSCs/iDPSCs therapy were assessed. The results showed that iDPSCs treatment increased Pax7 and MyoD mRNA expression, suggesting that iDPSCs were beneficial for the population of satellite cells and activated myogenic cells, respectively (Figures 6B and 6C). To further evaluate the renewal of satellite cells ($Ki67^{+}/Pax7^{+}$), immunofluorescence was used (Figure 6D). The results showed that the ratio of $Pax7^{+}/Ki67^{+}$ vs. $Pax7^{+}/Ki67^{-}$ cells decreased significantly in the cross-section of the genioglossus muscle in CIH mice. When treated with DPSCs or iDPSCs, the ratio of $Ki67^{+}/Pax7^{+}$ cells increased, with a greater increase observed with iDPSCs compared to DPSCs (Figure 6E). This indicates that stem cell therapy enhances the proliferation and renewal of satellite cells in CIH mice. To further explore the contribution of DPSCs/iDPSCs to upper airway repair in CIH mice, immunohistochemistry was performed using human-specific cytoplasmic proteins STEM121. STEM121 was only identified in the GG after iDPSCs, suggesting that iDPSCs directly participate in myogenic differentiation for GG repair in CIH mice (Figure 6F).

## DPSCs/iDPSCs help strengthen myotube formation in the DPSC-C2C12 direct and indirect coculture system under hypoxia in *vitro*

To explore the protective mechanism of DPSCs/iDPSCs, a direct co-culture of DPSCs/iDPSCs and C2C12 cells was performed, respectively (Figure 7A). Immunofluorescence staining of Desmin, hNu, and DAPI was performed. We found that C2C12 culture alone can form robust multinucleated myotubes under normoxia (Figure 7B first column). DPSCs cultured alone cannot induce cell fusion after 7 days (Figure 7B second column), whereas iDPSCs cultured alone appeared to initiate cell fusion into myotubes (Figure 7B third column). However, hypoxia disrupted this process, leading to cell atrophy (Figure 7B last two columns; Figure 7C last column). When cells were directly co-cultured, both DPSCs and iDPSCs were able to promote the formation of much thicker myotubes under hypoxia (Figure 7C third and fourth columns). It was observed that human nuclei (hNu) were incorporated into myotubes in iDPSCs-C2C12 coculture system (Figure 7C third column). While no fused hNu was found in DPSCs-C2C12 coculture system (Figure 7C fourth column), quite different when they were co-cultured under normoxia (Figure 7C second column). This revealed that DPSCs/iDPSCs can promote myogenic differentiation under hypoxia. iDPSCs participate in myogenic differentiation, with human-derived nuclei incorporated into the newly regenerated muscles, while DPSCs may have an effect through other mechanisms.

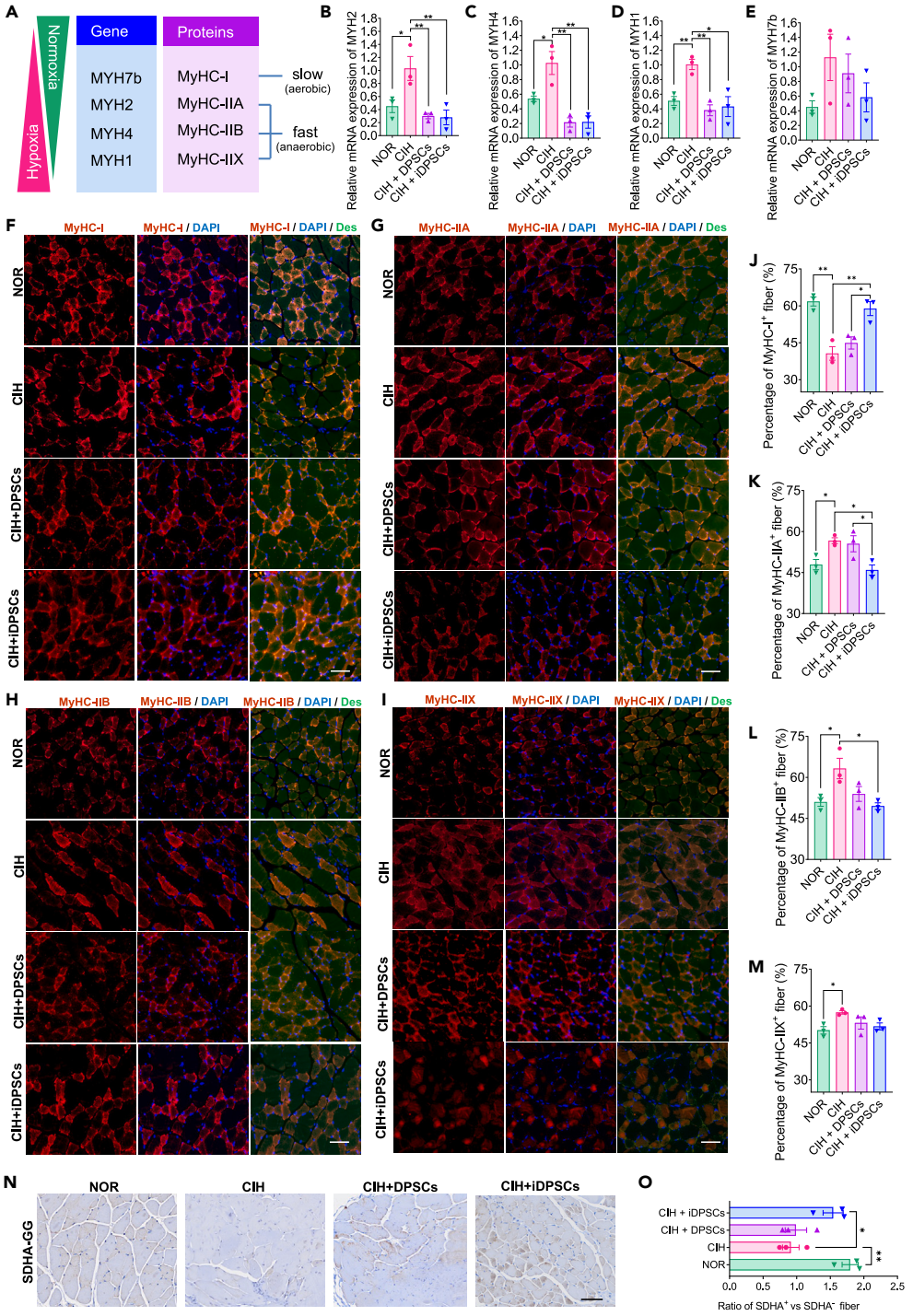


**Figure 3. DPSCs therapy can reduce the expression level of fast muscle fiber in GG tissue**

(A) MYH genes were displayed with the corresponding protein products, muscle twich pattern, and metabolic features. Slow-twich (aerobic) muscle fiber MyHC-I, and fast-twitch (anaerobic) muscle fiber MyHC-IIA, MyHC-IIB, and MyHC-IIX are encoded by MYH7b, MYH2, MYH4, and MYH1, respectively. Hypoxia promotes slow to fast fiber-type transition, while normoxia brings fast to slow fiber-type transition.

(B–E) Relative mRNAs of (B) MYH2, (C) MYH4, (D) MYH1, and (E) MYH7b in GG were assessed using quantitative PCR. Data are shown as mean ± SEM, $n = 3$, Student's t test for NOR vs. CIH, one-way ANOVA for CIH vs. CIH + DPSCs vs. CIH + iDPSCs by Fisher's LSD test for multiple comparison, $^{*}p < 0.05$, $^{**}p < 0.01$.

(F–I) Slow fibers were identified by MyHC-I (F), and fast fibers were identified by MyHC-IIA (G), MyHC-IIB (H), and MyHC-IIX (I) in GG using immunofluorescence staining. They were co-expression with Nuclei (DAPI) and fiber basement (Des, Desmin). Scale bar, 50 μm.

**Figure 3. *Continued***

(J–M) Quantitative analysis of MyHC-I (J), MyHC-IIA (K), MyHC-IIX (L), and MyHC-IIB (M)-positive fiber in GG cross sectional area was conducted, showing the fast-to-slow fiber-type transition under iDPSCs treatment. Data are shown as mean ± SEM, $n = 3$, Student's t test for NOR vs. CIH, One-way ANOVA for CIH vs. CIH + DPSCs vs. CIH + iDPSCs by Fisher's LSD test for multiple comparison, $^{*}p < 0.05$, $^{**}p < 0.01$.

(N) Mitochondrial activity levels were measured by immunohistochemistry of succinate dehydrogenase (SDHA) staining in GG, stand for slow-twitch (aerobic) fibers. Scale bar, 50 μm.

(O) Quantitative analysis of $DSHA^{+}$ vs. $DSHA^{-}$ fiber cross sectional area, stand for the ratio of slow-twitch (aerobic) fibers against fast twitch (anaerobic) fibers. Data are shown as mean ± SEM, $n = 3$, Student's $t$ for NOR vs. CIH, One-way ANOVA for CIH vs. CIH + DPSCs vs. CIH + iDPSCs by Fisher's LSD test for multiple comparison, $^{*}p < 0.05$.

Our pilot study tested the paracrine effects of DPSCs to protect myoblasts under hypoxia *in vitro*.[26] Therefore, the conditioned medium of DPSCs/iDPSCs was used to further explore the paracrine effect of DPSCs/iDPSCs under hypoxia, respectively (Figure 7A). We found that both DPSCs and iDPSCs can promote the formation of much thicker myotubes under hypoxia (Figure 7D). This revealed both DPSCs and iDPSCs can promote myogenic differentiation through paracrine effects.

### iDPSCs protect myoblasts under hypoxia by transcriptionally increasing myogenic gene expression

To determine whether iDPSC nuclei merged in mouse hybrid myotubes can contribute to muscle-specific gene expression, we detected sequential expression of human and/or mouse muscle transcripts, such as Pax7, MyoD, and Desmin, in C2C12-DPSC/iDPSCs co-cultures. Therefore, the relative mRNA expression levels of hMyoD, hPax7, and hDesmin (human source) and mMyoD, mPax7, and mDesmin (mouse source) were measured. The results showed that on the 4th day, the mRNA expression of hPax7 in the iDPSCs group was lower than that in the DPSCs group (Figure 7E). However, the mRNA expression of hMyoD was higher in the iDPSC group than in the DPSC group (Figure 7F), indicating that iDPSCs accelerated the myogenic process compared to DPSCs. No significant differences were found in mPax7 and mMyoD expression (Figures 7G and 7H). The mRNA expression of hDesmin and mDesmin in the iDPSC group also increased more than that in the DPSC groups on the 4th and 5th days (Figures 7I and 7J), suggesting that iDPSCs significantly enhanced the formation of myotube-like cells. These results suggest that the potential myogenic repair of iDPSCs under hypoxia may be related to increased transcription of myogenic genes.

## DISCUSSION

In our study, DPSCs/iDPSCs grafts *in vivo* improved $EMG^{GG}$ and muscle fiber type transition, diet and body weight, and decreased levels of TNF-α, ALT, LDH, and CK in CIH mice, all of which were more pronounced in the iDPSC groups. This indicates that DPSCs/iDPSCs grafts have both local and systemic actions, but the specific mechanism is unclear. We found iDPSCs promote myogenic repair by elevating MyoD and Pax7 expression and increasing the ratio of $Ki67^{+}/Pax7^{+}$ cells of GG in CIH mice. iDPSCs directly participate in muscle regeneration, as human-derived cytoplasmic proteins STEM121 can be identified in the regenerated muscles after iDPSCs grafts. Moreover, C2C12-DPSCs/iDPSCs co-culture or conditional medium of DPSCs/iDPSCs to C2C12 systems were established to explore their protective effects under hypoxia *in vitro*. The results revealed that both DPSCs and iDPSCs can promote muscle regeneration through paracrine effects. iDPSCs can participate in myogenic differentiation, by fusing human-derived nuclei and increasing human-derived myogenic transcripts. These findings provide the experience foundation for the treatment of OSA with DPSCs.

Generally, muscle contraction is regulated in two main ways: (1) by the number of motor units (amplitude) and (2) by the frequency of motor units (frequency).[27] Animal experiments have shown that CIH can alter the motion control of the hypoglossal nucleus by reducing the amplitude and frequency of genioglossus (GG) motor units.[28] The contractility of the GG are reduced in OSA patients or CIH animals.[3,29] In our study, we observed that both DPSCs and iDPSCs transplantation enhanced GG function by increasing the amplitude and frequency of $EMG^{GG}$, especially in the iDPSCs group (Figure 2). Ray et al. transplanted induced myogenic progenitor cells into damaged muscles and observed enhanced muscle contraction strength. It is highly related to newly generated muscle fibers with motion units innervating.[30] Therefore, we speculate that DPSCs/iDPSCs may promote muscle regeneration, thereby enhancing EMG.

Muscle regeneration goes through the process: satellite cells being activated, myogenic differentiation into myotubes, and finally developing into fibers. In general, fiber maturation involves a sequential expression of MyHC: MyHC-I (MYH7b), MyHC-IIA (MYH2), and MyHC-IIB (MYH4)/MyHC-IIX (MYH1).[23] This process is similar to embryonic myogensis, with time-dependent expression of MyHCs: A significant proportion of slow MyHC-I fibers during the first postnatal week are subsequently transformed into fast MyHC fibers during the first 1–4 postnatal weeks.[31] Two weeks after stem cell transplantation, MYH7b completes transcription (no significant differences can be found in mRNA expression of MYH7b) and gives rise to the expression of MyHC-I. iDPSCs have a more rapid effect on MyHC-I protein levels. We speculate that stem cells may initially promote the regeneration of slow-switch muscle fibers. Incitti T et al. transplant myogenic-induced pluripotent stem cells into dystrophic mice and also found PSC-derived myofibers express slow and oxidative myosin heavy-chain isoforms.[32] Next, this newly formed muscle began to progressively transition to fast-twitch fibers. Notably, there are two key triggers for muscle fiber transitions: repeated high-level muscle activity or exposure to hypoxia.[33,34] It is now believed that hypoxia (oxygen levels) is the primary cause of muscle fiber transitions.[34] In our study, we speculated that the enhanced $EMG^{GG}$ may result in oxygen inhalation during the non-CIH phase or reoxygenation period, resulting in a decrease in fast muscle fibers. This decreased fast muscle fiber transitions is considered a primary adaptation to increased oxygen content resulting from enhanced muscle strength, rather than a pathological change due to high-level muscle vibration.[35]

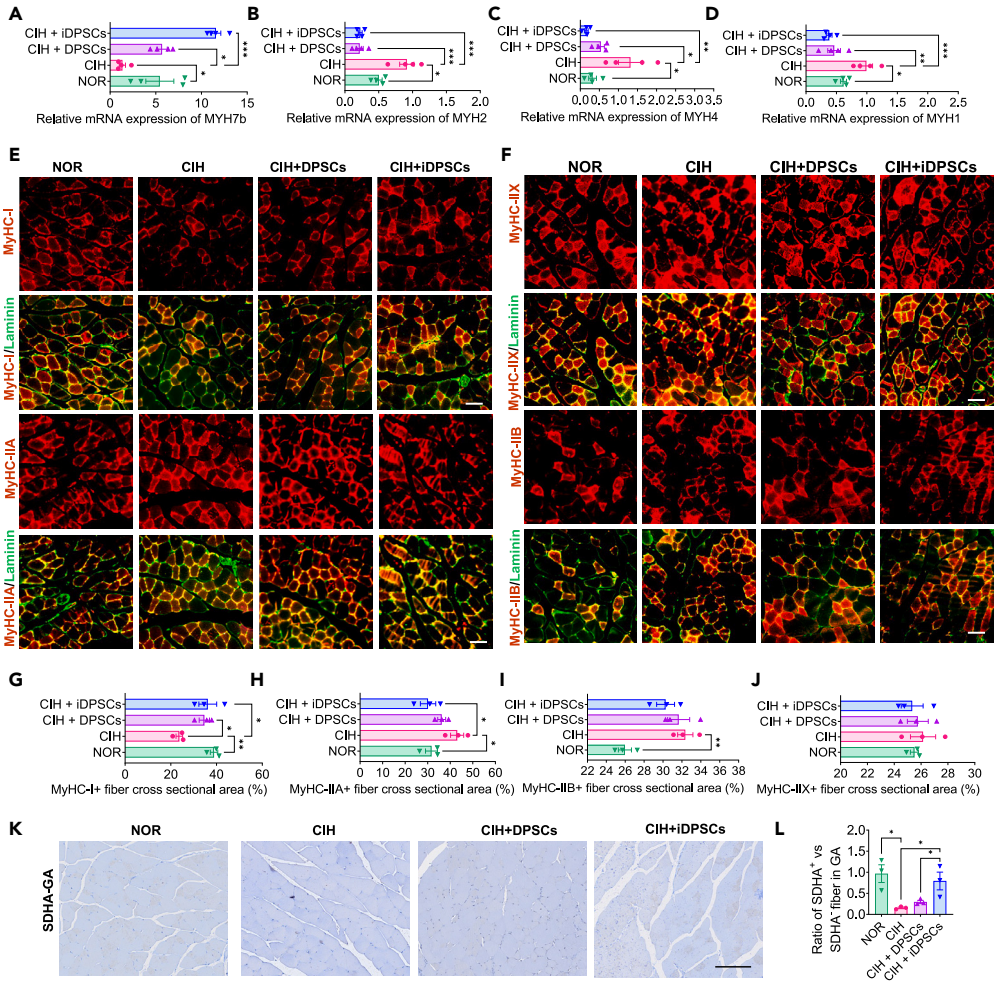


**Figure 4. DPSCs therapy can increase the ratio of fast to slow twitch muscle fibers in gastrocnemius muscle**

(A–D) Relative mRNAs of (A) MYH7b, (B) MYH2, (C) MYH4, and (D) MYH1 in GA were assessed using quantitative PCR. Data are shown as mean ± SEM, $n = 4$, Student's t test for NOR vs. CIH, one-way ANOVA for CIH vs. CIH + DPSCs vs. CIH + iDPSCs by Fisher's LSD test for multiple comparison, $^{*}p < 0.05$, $^{**}p < 0.01$.

(A and B) Slow fibers were identified by MyHC-I (E), and fast fibers were identified by MyHC-IIA (E), MyHC-IIX and MyHC-IIB (F) in GA using immunofluorescence staining. They were co-expression with fiber outline (Laminin). Scale bar, 50 μm.

(G–J) Quantitative analysis of MyHC-I (G), MyHC-IIA (H), MyHC-IIX (I), and MyHC-IIB (J)-positive fiber in GA cross-sectional area. Data are shown as mean ± SEM, $n = 3$, Student's t test for NOR vs. CIH, one-way ANOVA for CIH vs. CIH + DPSCs vs. CIH + iDPSCs by Fisher's LSD test for multiple comparison, $^{*}p < 0.05$, $^{**}p < 0.01$.

(K) Mitochondrial activity levels were measured by immunohistochemistry of succinate dehydrogenase (SDHA) staining in GA, stand for slow-twitch (aerobic) fibers. Scale bar, 100 μm.

(L) Quantitative analysis of $DSHA^{+}$ vs. $DSHA^{-}$ fiber cross-sectional area, stand for the ratio of slow-twitch (aerobic) fibers against fast twitch (anaerobic) fibers. Data are shown as mean ± SEM, $n = 3$, Student's t test for NOR vs. CIH, one-way ANOVA for CIH vs. CIH + DPSCs vs. CIH + iDPSCs by Fisher's LSD test for multiple comparison, $^{*}p < 0.05$.

Similar to upper airway muscles, DPSCs/iDPSCs therapy can increase the proportion of slow type I fibers and aerobic respiration in GA. This may be due to the enhanced GG function in response to increased oxygen inhalation, or the systemic action by DPSCs/iDPSCs grafts.

CIH, a hallmark of OSA, is linked to the onset of various systemic complications, such as cardiovascular disease, metabolic disorders, and hepatic injury, etc.[36] CIH disrupted food intake and water consumption, leading to a restriction in body weight.[37] To further investigate the systemic effects of DPSCs/iDPSCs treatment, the aforementioned conditions have been assessed. DPSCs/iDPSCs transplantation improved body weight in CIH mice. Exposure to CIH of mice, notably, the weight loss associated with CIH may be attributed to interference with diet.[38] In our study, the trend of changes in food intake and water consumption of mice was similar to that of body weight, supporting the previous suspicion that body weight loss was related to the reduction in food intake in CIH mice.[39] In addition, weight loss due to CIH exposure may be related to metabolic dysfunction, thus inducing chronic liver injury by increasing the levels of ALT and AST.[40] In our study, stem cell therapy significantly reduced the level of ALT. The level of ALT was directly proportional to the severity of hypoxia stimulation, and oxygen supply

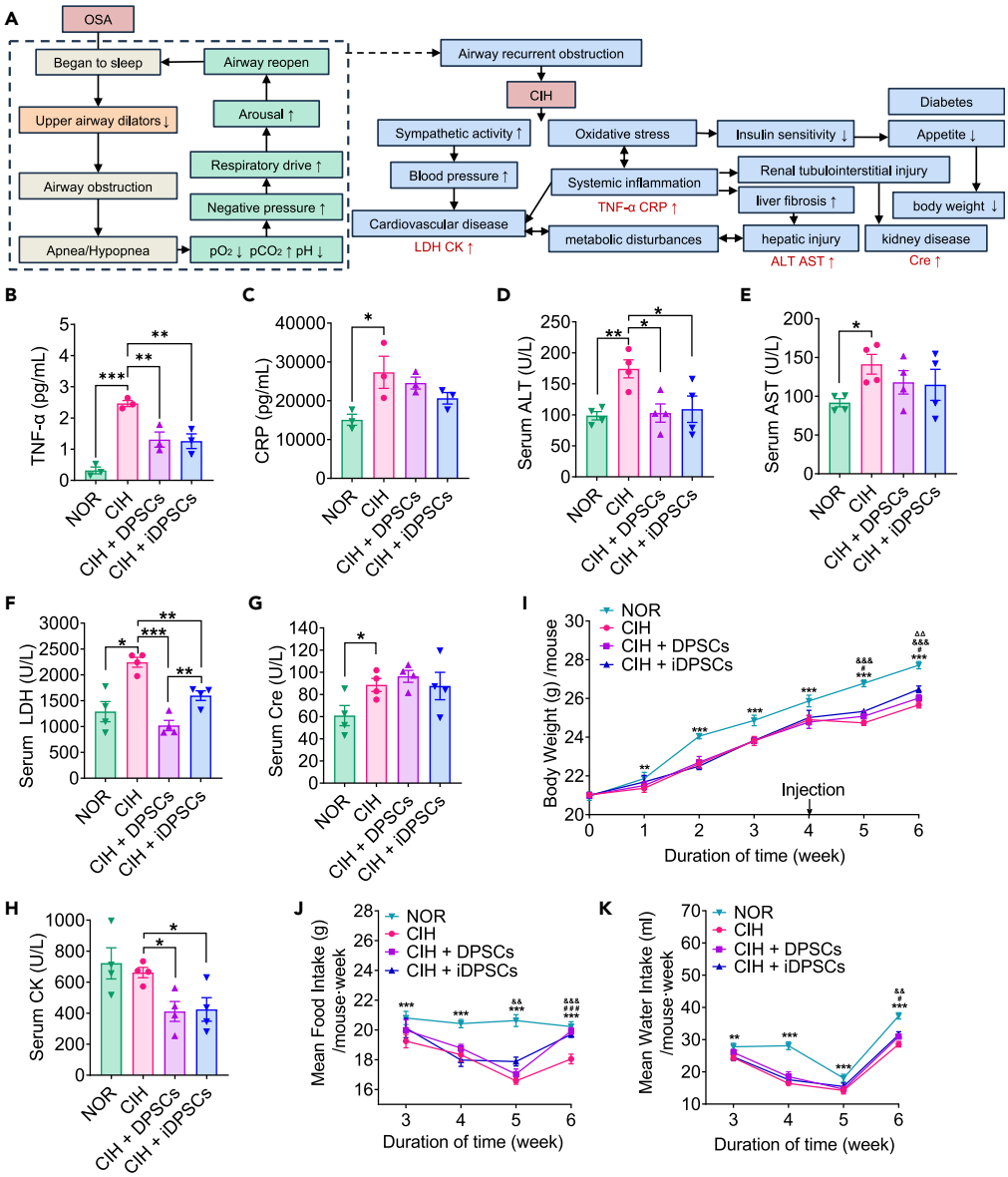


**Figure 5. DPSCs transplantation improved systemic complications in CIH mice**

(A) Pathological mechanisms of OSA and its complication. The activity of upper airway dilators in OSA patients decreased at sleep, resulting in airway obstruction. In this case, carbon dioxide, negative pressure and respiratory drive continue to increase until arousal, then the airway reopened. CIH caused by the airway recurrent obstruction would induce sympathetic activation, oxidative stress and systemic inflammation (elevated TNF-α and CRP), thereby cause blood pressure surges and metabolic disturbance, consequently, developing to cardiovascular disease (elevated LDH and CK), hepatic injury (elevated AST and ALT), and kidney disease (elevated Cre), etc. Additionally, appetite disturbed by metabolic problems might bring to body weight changes.

(B and C) Plasma levels of TNF-α (B) and CRP (C) were assessed by Elisa after DPSCs/iDPSCs treatment at the end of sixth week. Data are shown as mean ± SEM, $n = 3$, Student's t test for NOR vs. CIH, One-way ANOVA for CIH vs. CIH + DPSCs vs. CIH + iDPSCs by Fisher's LSD test for multiple comparison, $^{*}p < 0.05$, $^{**}p < 0.01$, $^{***}p < 0.001$.

(D–H) Serum levels of ALT (D), AST (E), LDH (F), Cre (G), and CK (H) were assessed after DPSCs/iDPSCs treatment at the end of sixth week. Data are shown as mean ± SEM, $n = 4$, Student's t test for NOR vs. CIH, one-way ANOVA for CIH vs. CIH + DPSCs vs. CIH + iDPSCs by Fisher's LSD test for multiple comparison, $^{*}p < 0.05$, $^{**}p < 0.01$, $^{***}p < 0.001$.

(I) Body weight changes during the six-week CIH exposure accompanied with DPSCs/DPSCs or Saline control injection at the end of fourth week.

(J and K) Mean food intake (J) and water intake (K) changes per mouse·week were also measured for the last four week. Data are shown as mean ± SEM, $n = 6$, two-way ANOVA by Fisher's LSD test for multiple comparison, CIH vs. NOR $^{**}p < 0.01$, $^{***}p < 0.001$; DPSCs vs. CIH $^{\#}p < 0.05$, $^{\#\#\#}p < 0.001$; iDPSCs vs. CIH $^{\&\&}p < 0.01$, $^{\&\&\&}p < 0.001$; iDPSCs vs. DPSCs $^{\Delta\Delta}P < 0.01$. TNF-α, tumor necrosis factor alpha; CRP, C-reactive protein; ALT, alanine aminotransferase; AST, aspartate aminotransferase; LDH, lactate dehydrogenase; Cre creatinine; CK, creatine kinase.

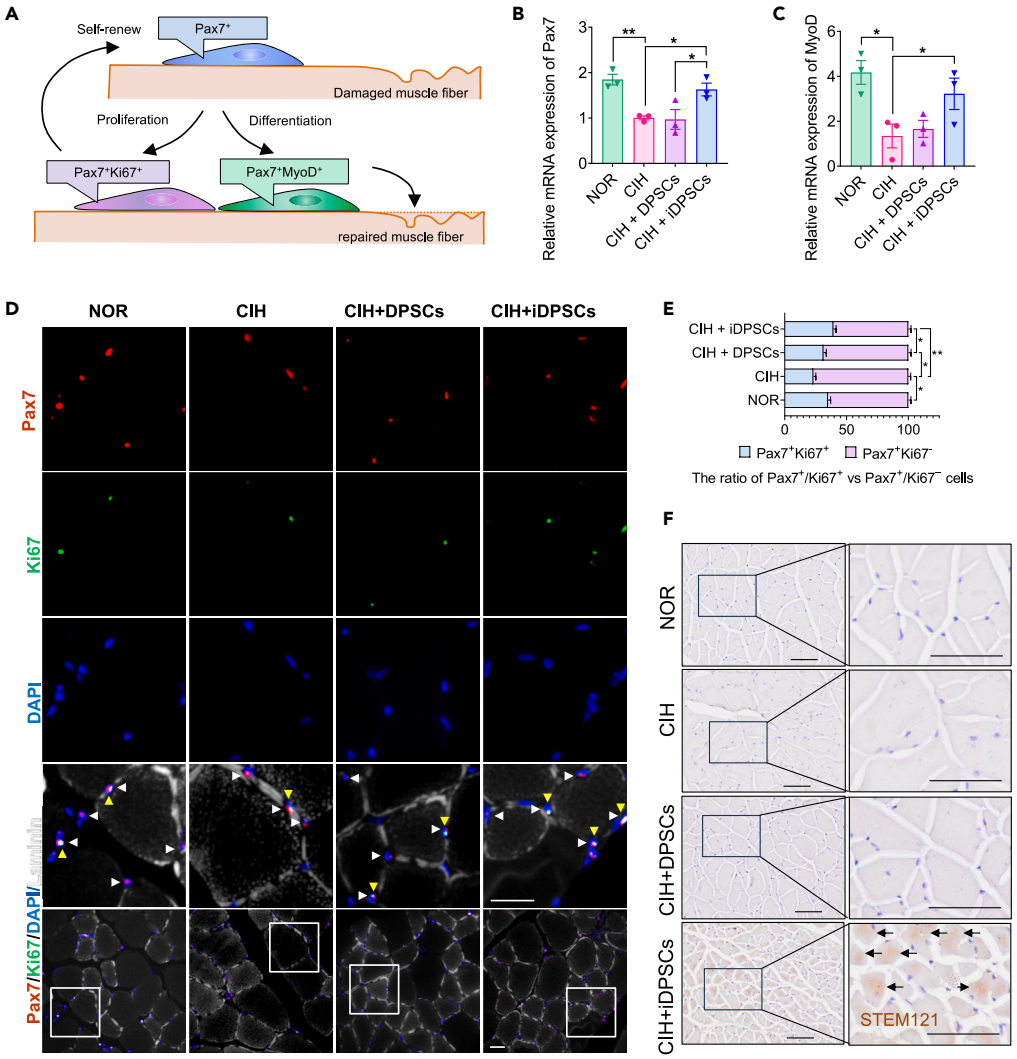


**Figure 6. iDPSCs promote muscle rengeration of GG in CIH mice**

(A) Schematic diagram of muscle regeneration: satellite cells ($Pax7^+$) are activated to proliferate ($Ki67^+$) and differentiated to myoblast ($MyoD^+$) for muscle repair, while another subset achieve self-renewal.

(B and C) mRNA expression level of Pax7 (B) and MyoD (C) in GG in CIH mice after DPSCs/iDPSCs treatment at the end of sixth week. Data are shown as mean ± SEM, $n = 3$, Student's test for NOR vs. CIH, One-way ANOVA for CIH vs. CIH + DPSCs vs. CIH + iDPSCs by Fisher's LSD test for multiple comparison, $*p < 0.05$, $**p < 0.01$ (D) Pax7(red) and Ki67 (green) co-immunostaining of GG cross-sections in CIH mice. Nuclei are counterstained with DAPI. Laminin staining is shown in white in the merged image. Scale bar, 20 μm. White arrowheads indicate only $Pax7^+$ cells. Yellow arrowheads indicate $Pax7^+/Ki67^+$cells.

(E) The ratio of $Pax7^+/Ki67^+$ vs. $Pax7^+/Ki67^-$ cells from all groups is represented as a bar graph. Data are shown as mean ± SEM, $n = 3$, Student's t test for NOR vs. CIH, One-way ANOVA for CIH vs. CIH + DPSCs vs. CIH + iDPSCs by Fisher's LSD test for multiple comparison, $*p < 0.05$, $**p < 0.01$.

(F) Human-derived cytoplasmic proteins (STEM121) were only identified in GG after iDPSCs treatment using immunohistochemistry. The arrows indicate Stem121-positive cells. Scale bar, 50 μm.

restored it to normal levels.[8] Intravenously administered with DPSCs can improved body weight in mice by regulating glucose and lipid metabolism in liver.[41] DPSCs transplantation improved body weight in a mouse chronic obstructive pulmonary disease model by regulating inflammation.[42] In our study, DPSCs/iDPSCs protect against cardiac injury by reducing the levels of LDH and CK, thereby improving the metabolic status and hypoxia condition. Conditioned medium from DPSCs reduced myocardial infarct size as well as decreased inflammatory factors in a mouse model of ischemia-reperfusion.[43] These changes may be regulated by systemic inflammation induced from CIH.[6] Transplanting DPSCs intramuscularly showed better improvement in body weight with a reduction in TNF-α and CRP levels in the blood plasma.[44] We found that DPSCs/iDPSCs can reduce TNF-α levels in CIH mice. This is in line with earlier reports demonstrating the anti-inflammatory effects of MSC transplantation in OSA-rats.[45] Therefore, we speculate that DPSCs/iDPSCs help promote systemic amelioration in CIH mice by reducing

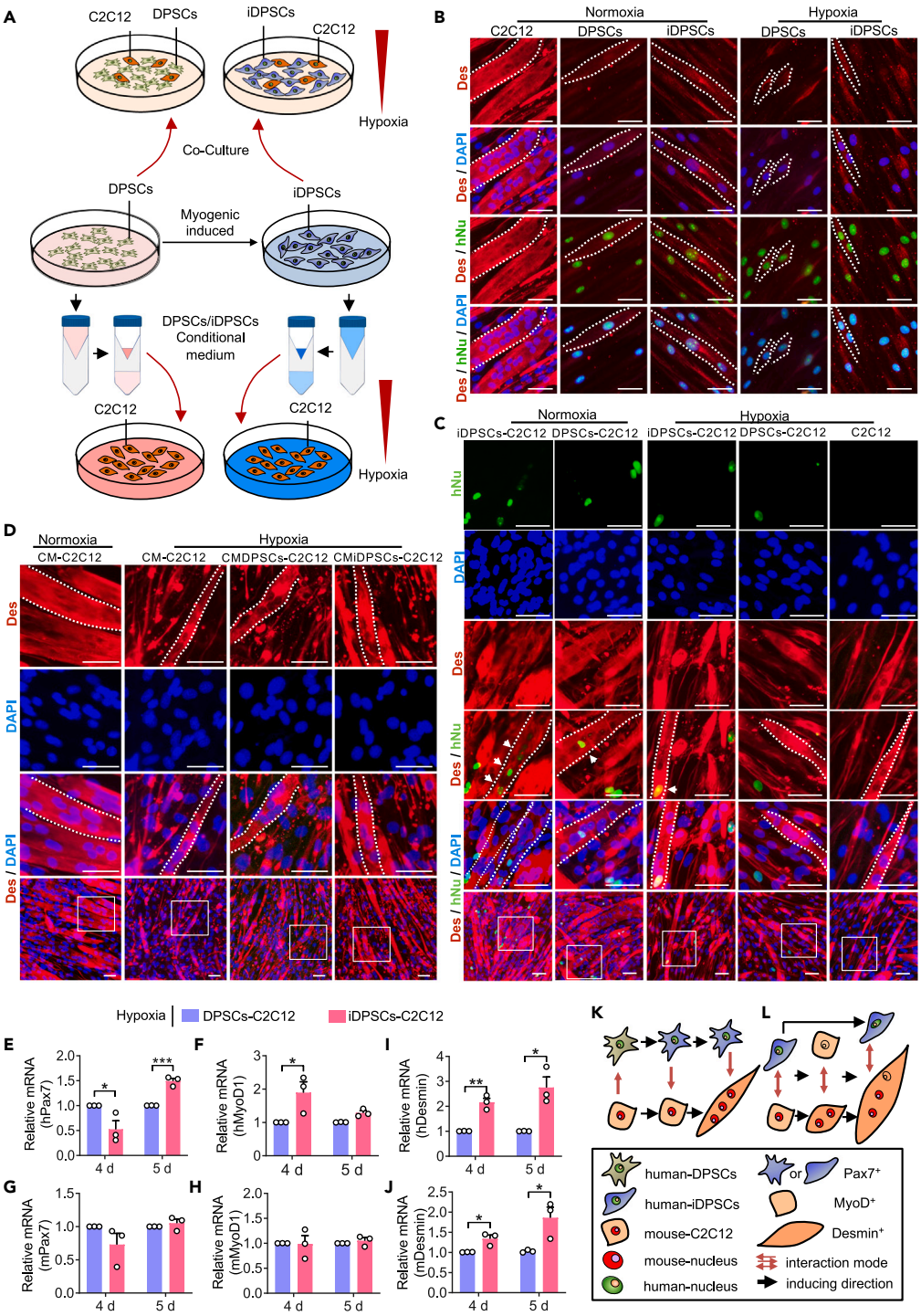


**Figure 7. iDPSCs help strengthen myogenic repair in co-culture system under hypoxia *in vitro***

(A) Schematic diagram of C2C12-DPSCs/iDPSCs co-culture system under hypoxia. DPSCs were myogenic induced into iDPSCs. C2C12 are directly co-cultured with DPSCs or iDPSCs under hypoxia for 7 days (above). C2C12 are also cultured with CM-DPSCs or CM-DPSCs under hypoxia for 7 days (below).

(B) Immunofluorescence staining with Desmin (red), hNu (green), and DAPI (blue) in cultured alone cells. White dotted line outlined the cells' morphology. Scale, 50 μm.

(C) Immunofluorescence staining with Desmin (red), hNu (green), and DAPI (blue) in direct co-culture system. White dotted line indicated the outline of multinucleated myotube cell. White arrow indicated fused hNu in Desmin$^{+}$ myotube cells. Scale, 50 μm.

**Figure 7. *Continued***

(D) Immunofluorescence staining with Desmin (red) and DAPI (blue) shows multinucleated myotube and nuclei in C2C12 culture with condition medium of DPSCs/iDPSCs (CMDPSCs/CMiDPSCs). White dotted line indicated the outline of multinucleated myotube. Scale, 50 μm.

(E–J) The levels of relative mRNAs, including (E) hPax7, (F) hMyoD, (G) mPax7, (H) mMyoD, (I) hDesmin, and (J) mDesmin. Data are shown as mean ± SEM, $n = 3$, Student's t test, *$p < 0.05$, **$p < 0.01$, ***$p < 0.001$.

(K and L) Schematic diagram of the mechanism of DPSCs (K) and iDPSCs (L) protect myoblast under hypoxia *in vitro*. (K) Under the influence of C2C12, DPSCs initially expressed $hPax7^+$, later promoted C2C12 myotubes ($mDesmin^+$) by paracrine effects.

(L) Provided with previously induced to $Pax7^+$ cells, some iDPSCs accelerated myogenic differentiation to $hPax7^-hMyoD^+$, while others were preserved ($hPax7^+$). This in turn hastened the fusion of C2C12 ($mDesmin^+$) by paracrine effects. Then some iDPSCs continued to differentiate with human/mouse nuclei fused into myotubes ($hDesmin^+$ and $mDesmin^+$), while others still retained $hPax7^+$ by self-renewal.

systemic inflammation to provide an anti-inflammatory microenvironment, thus improve liver metabolism and cardiac function, ultimately leading to weight gain.

At present, the main effects of MSCs in treating OSA/CIH are committed differentiation and paracrine effects (for example, secreting multiple proangiogenic, antiapoptotic, or anti-inflammatory factors).[46,47] Systemic treatment with DPSCs has been shown to regulate inflammation to treat Duchenne muscular dystrophy.[48] DPSCs have demonstrated anti-fibrotic and immunomodulatory properties to interact with the surrounding microenvironment and strongly support their contribution to tissue regeneration.[49] In addition, DPSCs showed pronounced immunosuppressive activity, and can be used in animal models without immunosuppression.[16,50] This can be explained that DPSCs respond to systemic inflammation and secrete immunomodulatory factors (PDL1, FasL) that inhibit T cell activity, thus reducing immune attacks on self-tissues.[51,52] DPSCs can ameliorate sciatic nerve conduction velocity when administered into unilateral hindlimb skeletal muscles, and the efficacy is mainly attributed to the multiple secretomes secreted from transplanted DPSCs.[53] $GFP^+$ DPSCs can repair myocardial infarction when injected intramyocardially, with no histologic evidence of $GFP^+$ muscle cells within the infarct.[54] This suggests that DPSCs mainly secrete factors rather than directly differentiate to repair. We then tested the effects of conditioned medium from DPSCs or iDPSCs, and found that both DPSCs and iDPSCs can promote myogenic differentiation through paracrine effects. Furthermore, we tested the effects of iDPSCs under hypoxia *in vitro* and *in vivo*. Pisciotta et al. transplanted myogenic-induced DPSCs by 5-Aza into the gastrocnemius muscle of mdx/SCID mice and observed muscle regeneration.[19] In our study, we found that iDPSC transplantation increased the expression of Pax7 in tissues, which was beneficial to the muscle satellite cell population (Figures 6B, 6D, and 6E). Additionally, human-derived cytoplasmic proteins STEM121 were identified in GG after iDPSC treatment (Figures 5E and 5F). Some scholars also tested human-specific hNu, hLaminin, or $hPax7^+$ in muscle fibers,[55,56] indicating that induced myogenic cells were stably transplanted *in vivo* and contributed to the muscle satellite cell pool.

We further verified through coculture *in vitro* that both DPSCs and iDPSCs promoted the formation of myotubes. Specifically, nuclei derived from iDPSCs fused into the myotubes formed under hypoxia. Similar to our findings, both human and mouse nuclei were observed in newly formed hybrid myotubes when coculturing DPSCs with C2C12 cells.[19,57] Grabowska et al. cocultured umbilical cord blood MSCs with C2C12 cells. On the seventh day, myotube-like cells were arranged. On the ninth day, approximately 15% of all formed myotubes were hybrid myotubes containing human nuclei.[58] Direct coculture system was shown to promote stronger myotubes compared to the conditioned medium system. This resembles the result that direct cocultures can better drives DPSCs toward smooth muscle cells differentiation.[59] We speculate that direct contact with cells forces DPSCs/iDPSCs to contribute to myogenic differentiation (through fusion with human-derived nuclei) in addition to paracrine effects under normoxia. However, hypoxia disrupted this process, resulting in fusion of only iDPSCs-derived nuclei. Yuchen Zhang et al. also found that direct cocultures with endothelial cells significantly drive DPSCs toward smooth muscle cell differentiation compared to indirect cocultures.[59] This indicates that direct cocultures can drive committed differentiation apart from paracrine action when compared to indirect cocultures. As a potential source of cells to help in the regeneration of functioning muscle tissue, it is important that fused nuclei be able to produce muscle-specific transcripts from donor sourse.[60] Milner et al. found increased myogenic transcripts from mouse or pig sources by co-culturing porcine adipose MSCs with mouse C2C12 cells, verifying that the nuclei incorporated into myotubes are functioning myonuclei.[61] In our study, we observed sequential alterations in myogenic transcripts and speculated on the protective mechanism of DPSCs/iDPSCs (Figures 7K and 7L). When compared with DPSCs, iDPSCs increased the levels of Desmin, Pax7, and MyoD from human sources. This suggests that iDPSCs promote myotubes through both paracrine effects and myogenic committed differentiation.

## Conclusion

In our study, DPSCs/iDPSCs therapy *in vivo* enhances GG function by promoting muscle repair and reducing inflammatory factors. This improvement leads to enhanced systemic condition and body weight, resulting in muscle fiber transition in the upper airway and lower limb muscles. Moreover, iDPSCs grafts increased the proportion of $Pax7^+/Ki67^+$ and human-derived cells in the GG of CIH mice compared with DPSCs and were beneficial to the $Pax7^+$ satellite cell pool for muscle repair *in vitro* and *in vivo*. Apart from the paracrine effect similar to DPSCs, iDPSCs participate in myogenic differentiation, with the human-derived nucleus being incorporated into the newly regenerated muscles. These data provide the experiment foundation for the treatment of OSA with DPSCs.

## Limitations of the study

This study applied myogenic induced DPSCs to treat GG injury in CIH mice. An important limitation of the study was not differentiated donor gender in cell use and the exclusive use of male recipient mice. It is possible that cells from different donor sources might exhibit heterogeneity issues and also might have different effect on female mice. Future research should differentiate the impact of gender/sex on

experimental outcomes. Notably, the CIH model was aimed at studying GG injury in CIH pathological state as OSA consequence. DPSCs/iDPSCs therapy can improve muscle regeneration and GG function, but this can only increase oxygen inhalation during the non-CIH phase or reoxygenation period. It cannot be verified that the state of CIH has been altered. In the future, spontaneous OSA animal models can be used to validate stem cell therapy, with blood oxygen saturation and sleep monitoring. Besides, GG located in deep intramuscular position. Therefore, there are some difficulties in clinical application, although this GG injection can be trained to ensure accuracy. The future work aims to identify intraoral landmarks for precise administration in GG of OSA patients. It can be achieved by combining the modification of a computer-controlled local drug delivery system, which allows drugs to enter tissues at a very precise pressure/flow ratio and precise dosage, with reduced injection pain. This provides basis for clinical appliance of stem cells or other drugs to treat OSA patients.

## RESOURCE AVAILABILITY

### Lead contact

Additional information and requests for resources and reagents used in this study should be directed to and will be fulfilled by the lead contact, Yue-Hua Liu (liuyuehua@fudan.edu.cn).

### Materials availability

This study did not generate new unique reagents.

### Data and code availability

- This paper analyzes existing, publicly available data. These accession numbers for the datasets are listed in the key resources table.
- Requests for original code should be directed to the corresponding authors.
- Any additional information required to reanalyze the data reported in this paper is available from the lead contact upon request.

## ACKNOWLEDGMENTS

This study was supported by National Key Research and Development Program of China (no. 2023YFC2509200), National Natural Science Foundation of China (81771109, 82271007), Natural Science Foundation of Shanghai (22ZR1454300), The Research and Development Project of Stomatology Hospital Zhejiang University School of Medicine (RD2022JCEL07, RD2023JCYL02). We thank everyone on our team for assisting with the preparation of this manuscript.

## AUTHOR CONTRIBUTIONS

Y.-H.L. and W.-H.D. conceived and designed the experiments. M.-H.Z., W.-H.Z., Y.L., and L.-M.Y. conducted experiments. M.-H.Z., W.-H.Z., Y.L., L.-M.Y., X.-X.H., Y.X., and M.-J.W. conducted data analysis and prepared the figures. M.-H.Z. and W.-H. Z. wrote and revised the manuscript. Y.-H L. and W.-H.D. reviewed and edited the manuscript. All authors read and approved the final manuscript. M.-H.Z. and W.-H.Z. contributed equally to this work.

## DECLARATION OF INTERESTS

The authors declare no competing interests.

## STAR★METHODS

Detailed methods are provided in the online version of this paper and include the following:

- KEY RESOURCES TABLE
- EXPERIMENTAL MODEL AND STUDY PARTICPANT DETAILS
  - DPSC culture
  - DSPC myogenic induction
  - Cell hypoxia model
  - Direct coculture system
  - Conditional medium (CM) of DPSCs/iDPSCs
  - CIH animal model and GG transplantation
- METHOD DETAILS
  - Electromyography of the genioglossus muscle ($EMG^{GG}$)
  - Serum biochemical index detection
  - ELISA experiments
  - Hematoxylin and eosin staining
  - Masson staining
  - Immunofluorescence
  - Immunohistochemistry staining
  - RNA extraction and reverse transcription-quantitative polymerase chain reaction (RT-qPCR)
  - Western blot analysis
- QUANTIFICATION AND STATISTICAL ANALYSIS

## SUPPLEMENTAL INFORMATION

Supplemental information can be found online at https://doi.org/10.1016/j.isci.2024.111143.

Received: October 24, 2023
Revised: August 25, 2024
Accepted: October 7, 2024
Published: October 10, 2024

## REFERENCES

1. Strohl, K.P. (2003). Con: sleep apnea is not an anatomic disorder. Am. J. Respir. Crit. Care Med. *168*, 271–273. https://doi.org/10.1164/rccm.2305016.
2. Mediano, O., Romero-Peralta, S., Resano, P., Cano-Pumarega, I., Sánchez-de-la-Torre, M., Castillo-García, M., Martínez-Sánchez, A.B., Ortigado, A., and García-Río, F. (2019). Obstructive Sleep Apnea: Emerging Treatments Targeting the Genioglossus Muscle. J. Clin. Med. *8*, 1754. https://doi.org/10.1164/rccm.201806-1109TR.
3. McSharry, D., O'Connor, C., McNicholas, T., Langran, S., O'Sullivan, M., Lowery, M., and McNicholas, W.T. (2012). Genioglossus fatigue in obstructive sleep apnea. Respir. Physiol. Neurobiol. *183*, 59–66. https://doi.org/10.1016/j.resp.2012.05.024.
4. Jordan, A.S., and White, D.P. (2008). Pharyngeal motor control and the pathogenesis of obstructive sleep apnea. Respir. Physiol. Neurobiol. *160*, 1–7. https://doi.org/10.1016/j.resp.2007.07.009.
5. Unnikrishnan, D., Jun, J., and Polotsky, V. (2015). Inflammation in sleep apnea: an update. Rev. Endocr. Metab. Disord. *16*, 25–34. https://doi.org/10.1007/s11154-014-9304-x.
6. Baguet, J.P., Barone-Rochette, G., Tamisier, R., Levy, P., and Pépin, J.L. (2012). Mechanisms of cardiac dysfunction in obstructive sleep apnea. Nat. Rev. Cardiol. *9*, 679–688. https://doi.org/10.1002/oby.23679.
7. Giampá, S.Q.C., Lorenzi-Filho, G., and Drager, L.F. (2023). Obstructive sleep apnea and metabolic syndrome. Obesity *31*, 900–911. https://doi.org/10.1038/nrcardio.2012.141.
8. Mesarwi, O.A., Loomba, R., and Malhotra, A. (2019). Obstructive Sleep Apnea, Hypoxia, and Nonalcoholic Fatty Liver Disease. Am. J. Respir. Crit. Care Med. *199*, 830–841. https://doi.org/10.1164/rccm.201806-1109TR.
9. Gleeson, M., and McNicholas, W.T. (2022). Bidirectional relationships of comorbidity with obstructive sleep apnoea. Eur. Respir. Rev. *31*, 210256. https://doi.org/10.1183/16000617.0256-2021.
10. Strollo, P.J., Jr., Soose, R.J., Maurer, J.T., de Vries, N., Cornelius, J., Froymovich, O., Hanson, R.D., Padhya, T.A., Steward, D.L., Gillespie, M.B., et al. (2014). Upper-airway stimulation for obstructive sleep apnea. N. Engl. J. Med. *370*, 139–149. https://doi.org/10.1056/NEJMoa1308659.
11. Zhang, M., Liu, Y., Liu, Y., Yu, F., Yan, S., Chen, L., Lv, C., and Lu, H. (2019). Effectiveness of oral appliances versus continuous positive airway pressure in treatment of OSA patients: An updated meta-analysis. Cranio *37*, 347–364. https://doi.org/10.1080/08869634.2018.1475278.
12. Fleury Curado, T., Oliven, A., Sennes, L.U., Polotsky, V.Y., Eisele, D., and Schwartz, A.R. (2018). Neurostimulation Treatment of OSA. Chest *154*, 1435–1447. https://doi.org/10.1016/j.chest.2018.08.1070.
13. Anitua, E., Troya, M., and Zalduendo, M. (2018). Progress in the use of dental pulp stem cells in regenerative medicine. Cytotherapy *20*, 479–498. https://doi.org/10.1016/j.jcyt.2017.12.011.
14. Bertani, G., Di Tinco, R., Bertoni, L., Orlandi, G., Pisciotta, A., Rosa, R., Rigamonti, L., Signore, M., Bertacchini, J., Sena, P., et al. (2023). Flow-dependent shear stress affects the biological properties of pericyte-like cells isolated from human dental pulp. Stem Cell Res. Ther. *14*, 31. https://doi.org/10.1038/nrcardio.2012.141.
15. Jo, Y.Y., Lee, H.J., Kook, S.Y., Choung, H.W., Park, J.Y., Chung, J.H., Choung, Y.H., Kim, E.S., Yang, H.C., and Choung, P.H. (2007). Isolation and characterization of postnatal stem cells from human dental tissues. Tissue Eng. *13*, 767–773. https://doi.org/10.1089/ten.2006.0192.
16. Kerkis, I., Ambrosio, C.E., Kerkis, A., Martins, D.S., Zucconi, E., Fonseca, S.A.S., Cabral, R.M., Maranduba, C.M.C., Gaiad, T.P., Morini, A.C., et al. (2008). Early transplantation of human immature dental pulp stem cells from baby teeth to golden retriever muscular dystrophy (GRMD) dogs: Local or systemic? J. Transl. Med. *6*, 35. https://doi.org/10.1186/1479-5876-6-35.
17. Ha, J., Bharti, D., Kang, Y.H., Lee, S.Y., Oh, S.J., Kim, S.B., Jo, C.H., Son, J.H., Sung, I.Y., Cho, Y.C., Morini, A.C., et al. (2021). Human Dental Pulp-Derived Mesenchymal Stem Cell Potential to Differentiate into Smooth Muscle-Like Cells In Vitro. BioMed Res. Int. *2021*, 8858412. https://doi.org/10.1155/2021/8858412.
18. Jiang, W., Wang, D., Alraies, A., Liu, Q., Zhu, B., Sloan, A.J., Ni, L., and Song, B. (2019). Wnt-GSK3β/β-Catenin Regulates the Differentiation of Dental Pulp Stem Cells into Bladder Smooth Muscle Cells. Stem Cell. Int. *2019*, 8907570. https://doi.org/10.1155/2019/8907570.
19. Pisciotta, A., Riccio, M., Carnevale, G., Lu, A., De Biasi, S., Gibellini, L., La Sala, G.B., Bruzzesi, G., Ferrari, A., Huard, J., and De Pol, A. (2015). Stem cells isolated from human dental pulp and amniotic fluid improve skeletal muscle histopathology in mdx/SCID mice. Stem Cell Res. Ther. *6*, 156. https://doi.org/10.1186/s13287-015-0141-y.
20. Chretien, F., Dreyfus, P.A., Christov, C., Caramelle, P., Lagrange, J.L., Chazaud, B., and Gherardi, R.K. (2005). In vivo fusion of circulating fluorescent cells with dystrophin-deficient myofibers results in extensive sarcoplasmic fluorescence expression but limited dystrophin sarcolemmal expression. Am. J. Pathol. *166*, 1741–1748. https://doi.org/10.1016/s0002-9440(10)62484-4.
21. Yang, B., Zheng, J.H., and Zhang, Y.Y. (2013). Myogenic differentiation of mesenchymal stem cells for muscle regeneration in urinary tract. Chin. Med. J. *126*, 2952–2959. https://doi.org/10.3760/cma.j.issn.0366-6999.20130508.
22. Kutzner, E.A., Miot, C., Liu, Y., Renk, E., Park, J.S., and Inman, J.C. (2017). Effect of genioglossus, geniohyoid, and digastric advancement on tongue base and hyoid position. Laryngoscope *127*, 1938–1942. https://doi.org/10.1002/lary.26380.
23. Schiaffino, S., and Reggiani, C. (2011). Fiber types in mammalian skeletal muscles. Physiol. Rev. *91*, 1447–1531. https://doi.org/10.1152/physrev.00031.2010.
24. McGuire, M., MacDermott, M., and Bradford, A. (2003). Effects of chronic intermittent asphyxia on rat diaphragm and limb muscle contractility. Chest *123*, 875–881. https://doi.org/10.1378/chest.123.3.875.
25. Song, S.O., He, K., Narla, R.R., Kang, H.G., Ryu, H.U., and Boyko, E.J. (2019). Metabolic Consequences of Obstructive Sleep Apnea Especially Pertaining to Diabetes Mellitus and Insulin Sensitivity. Diabetes Metab. J. *43*, 144–155. https://doi.org/10.4093/dmj.2018.0256.
26. Zhang, W., Yu, L., Han, X., Pan, J., Deng, J., Zhu, L., Lu, Y., Huang, W., Liu, S., Li, Q., and Liu, Y. (2020). The secretome of human dental pulp stem cells protects myoblasts from hypoxia-induced injury via the Wnt/β-catenin pathway. Int. J. Mol. Med. *45*, 1501–1513. https://doi.org/10.3892/ijmm.2020.4525.
27. Bailey, E.F. (2011). Activities of human genioglossus motor units. Respir. Physiol. Neurobiol. *179*, 14–22. https://doi.org/10.1016/j.resp.2011.04.018.
28. Edge, D., Bradford, A., Jones, J.F.X., and O'Halloran, K.D. (2012). Chronic intermittent hypoxia alters genioglossus motor unit discharge patterns in the anaesthetized rat. Adv. Exp. Med. Biol. *758*, 295–300. https://doi.org/10.1007/978-94-007-4584-1_40.
29. Zhang, M.H., Han, X.X., Lu, Y., Deng, J.J., Zhang, W.H., Mao, J.Q., Mi, J., Ding, W.H., Wu, M.J., Yu, L.M., and Liu, Y.H. (2023). Chronic intermittent hypoxia impaired collagen synthesis in mouse genioglossus via ROS accumulation: A transcriptomic analysis. Respir. Physiol. Neurobiol. *308*, 103980. https://doi.org/10.1016/j.resp.2022.103980.
30. Ray, A.D., Magalang, U.J., Michlin, C.P., Ogasa, T., Krasney, J.A., Gosselin, L.E., and Farkas, G.A. (2007). Intermittent hypoxia reduces upper airway stability in lean but not obese Zucker rats. Am. J. Physiol. Regul. Integr. Comp. Physiol. *293*, R372–R378. https://doi.org/10.1152/ajpregu.00038.2007.
31. DeNardi, C., Ausoni, S., Moretti, P., Gorza, L., Velleca, M., Buckingham, M., and Schiaffino, S. (1993). Type 2X-myosin heavy chain is coded by a muscle fiber type-specific and developmentally regulated gene. J. Cell Biol. *123*, 823–835. https://doi.org/10.1083/jcb.123.4.823.
32. Incitti, T., Magli, A., Jenkins, A., Lin, K., Yamamoto, A., and Perlingeiro, R.C.R. (2020). Pluripotent stem cell-derived skeletal muscle fibers preferentially express myosin heavy-chain isoforms associated with slow and oxidative muscles. Skeletal Muscle *10*, 17. https://doi.org/10.1186/s13395-020-00234-5.
33. Dahlin, L.B., and Lundborg, G. (2001). Vibration-induced hand problems: role of the peripheral nerves in the pathophysiology. Scand. J. Plast. ReConstr. Surg. Hand Surg.

*35*, 225–232. https://doi.org/10.1080/02844310175052312.
34. McGuire, M., MacDermott, M., and Bradford, A. (2002). The effects of chronic episodic hypercapnic hypoxia on rat upper airway muscle contractile properties and fiber-type distribution. Chest *122*, 1400–1406. https://doi.org/10.1378/chest.122.4.1400.
35. Pette, D., and Staron, R.S. (2001). Transitions of muscle fiber phenotypic profiles. Histochem. Cell Biol. *115*, 359–372. https://doi.org/10.1007/s004180100268.
36. Zhang, M., Lu, Y., Sheng, L., Han, X., Yu, L., Zhang, W., Liu, S., and Liu, Y. (2022). Advances in Molecular Pathology of Obstructive Sleep Apnea. Molecules *27*, 8422. https://doi.org/10.3390/molecules27238422.
37. Lüneburg, N., Siques, P., Brito, J., Arriaza, K., Pena, E., Klose, H., Leon-Velarde, F., and Böger, R.H. (2016). Long-Term Chronic Intermittent Hypobaric Hypoxia in Rats Causes an Imbalance in the Asymmetric Dimethylarginine/Nitric Oxide Pathway and ROS Activity: A Possible Synergistic Mechanism for Altitude Pulmonary Hypertension? Pulm. Med. *2016*, 6578578. https://doi.org/10.1155/2016/6578578.
38. Siques, P., Brito, J., Flores, K., Ordenes, S., Arriaza, K., Pena, E., León-Velarde, F., López de Pablo, Á.L., Gonzalez, M.C., and Arribas, S. (2018). Long-Term Chronic Intermittent Hypobaric Hypoxia Induces Glucose Transporter (GLUT4) Translocation Through AMP-Activated Protein Kinase (AMPK) in the Soleus Muscle in Lean Rats. Front. Physiol. *9*, 799. https://doi.org/10.3389/fphys.2018.00799.
39. do Carmo, J.M., da Silva, A.A., Moak, S.P., da Silva, F.S., Spradley, F.T., and Hall, J.E. (2019). Role of melanocortin 4 receptor in hypertension induced by chronic intermittent hypoxia. Acta Physiol. *225*, e13222. https://doi.org/10.1111/apha.13222.
40. Drager, L.F., Li, J., Reinke, C., Bevans-Fonti, S., Jun, J.C., and Polotsky, V.Y. (2011). Intermittent hypoxia exacerbates metabolic effects of diet-induced obesity. Obesity *19*, 2167–2174. https://doi.org/10.1038/oby.2011.240.
41. Ma, Y., Wang, L., Yang, S., Liu, D., Zeng, Y., Lin, L., Qiu, L., Lu, J., Chang, J., and Li, Z. (2021). The tissue origin of human mesenchymal stem cells dictates their therapeutic efficacy on glucose and lipid metabolic disorders in type II diabetic mice. Stem Cell Res. Ther. *12*, 385. https://doi.org/10.1186/s13287-021-02463-x.
42. Gao, X., Liu, Z., and Wang, Z. (2023). Dental Pulp Stem Cells Ameliorate Elastase-Induced Pulmonary Emphysema by Regulating Inflammation and Oxidative Stress. J. Inflamm. Res. *16*, 1497–1508. https://doi.org/10.2147/JIR.S402794.
43. Yamaguchi, S., Shibata, R., Yamamoto, N., Nishikawa, M., Hibi, H., Tanigawa, T., Ueda, M., Murohara, T., and Yamamoto, A. (2015). Dental pulp-derived stem cell conditioned medium reduces cardiac injury following ischemia-reperfusion. Sci. Rep. *5*, 16295. https://doi.org/10.1038/srep16295.
44. Datta, I., Bhadri, N., Shahani, P., Majumdar, D., Sowmithra, S., Razdan, R., and Bhonde, R. (2017). Functional recovery upon human dental pulp stem cell transplantation in a diabetic neuropathy rat model. Cytotherapy *19*, 1208–1224. https://doi.org/10.1016/j.jcyt.2017.07.009.
45. Ramos, P., Rubies, C., Torres, M., Batlle, M., Farre, R., Brugada, J., Montserrat, J.M., Almendros, I., and Mont, L. (2014). Atrial fibrosis in a chronic murine model of obstructive sleep apnea: mechanisms and prevention by mesenchymal stem cells. Respir. Res. *15*, 54. https://doi.org/10.1186/1465-9921-15-54.
46. Chen, M., Huang, Z., Bi, H., Pan, X., He, J., He, L., He, X., Du, J., Zhou, K., Wang, L., et al. (2019). Effects of bone marrow-derived mesenchymal stem cell transplantation on chronic obstructive pulmonary disease/obstructive sleep apnea overlap syndrome in rats. Mol. Med. Rep. *20*, 4665–4673. https://doi.org/10.3892/mmr.2019.10714.
47. Liang, L., Zheng, D., Lu, C., Xi, Q., Bao, H., Li, W., Gu, Y., Mao, Y., Xu, B., and Gu, X. (2021). Exosomes derived from miR-301a-3p-overexpressing adipose-derived mesenchymal stem cells reverse hypoxia-induced erectile dysfunction in rat models. Stem Cell Res. Ther. *12*, 87. https://doi.org/10.1186/s13287-021-02161-8.
48. Nitahara-Kasahara, Y., Kuraoka, M., Guillermo, P.H., Hayashita-Kinoh, H., Maruoka, Y., Nakamura-Takahasi, A., Kimura, K., Takeda, S., and Okada, T. (2021). Dental pulp stem cells can improve muscle dysfunction in animal models of Duchenne muscular dystrophy. Stem Cell Res. Ther. *12*, 78. https://doi.org/10.1186/s13287-020-02099-3.
49. Pisciotta, A., Di Tinco, R., Bertani, G., Orlandi, G., Bertoni, L., Pignatti, E., Orciani, M., Sena, P., Bertacchini, J., Salvarani, C., and Carnevale, G. (2023). Human dental pulp stem cells (hDPSCs) promote the lipofibroblast transition in the early stage of a fibro-inflammatory process. Front. Cell Dev. Biol. *11*, 1196023. https://doi.org/10.3389/fcell.2023.1196023.
50. de Mendonça Costa, A., Bueno, D.F., Martins, M.T., Kerkis, I., Kerkis, A., Fanganiello, R.D., Cerruti, H., Alonso, N., and Passos-Bueno, M.R. (2008). Reconstruction of large cranial defects in nonimmunosuppressed experimental design with human dental pulp stem cells. J. Craniofac. Surg. *19*, 204–210. https://doi.org/10.1097/scs.0b013e31815c8a54.
51. Zhao, Y., Wang, L., Jin, Y., and Shi, S. (2012). Fas ligand regulates the immunomodulatory properties of dental pulp stem cells. J. Dent. Res. *91*, 948–954. https://doi.org/10.1177/0022034512458690.
52. Di Tinco, R., Bertani, G., Pisciotta, A., Bertoni, L., Pignatti, E., Maccaferri, M., Bertacchini, J., Sena, P., Vallarola, A., Tupler, R., et al. (2021). Role of PD-L1 in licensing immunoregulatory function of dental pulp mesenchymal stem cells. Stem Cell Res. Ther. *12*, 598. https://doi.org/10.1186/s13287-021-02664-4.
53. Kanada, S., Makino, E., Nakamura, N., Miyabe, M., Ito, M., Hata, M., Yamauchi, T., Sawada, N., Kondo, S., Saiki, T., et al. (2020). Direct Comparison of Therapeutic Effects on Diabetic Polyneuropathy between Transplantation of Dental Pulp Stem Cells and Administration of Dental Pulp Stem Cell-Secreted Factors. Int. J. Mol. Sci. *21*, 6064. https://doi.org/10.3390/ijms21176064.
54. Gandia, C., Armiñan, A., García-Verdugo, J.M., Lledó, E., Ruiz, A., Miñana, M.D., Sanchez-Torrijos, J., Payá, R., Mirabet, V., Carbonell-Uberos, F., et al. (2008). Human dental pulp stem cells improve left ventricular function, induce angiogenesis, and reduce infarct size in rats with acute myocardial infarction. Stem Cell. *26*, 638–645. https://doi.org/10.1634/stemcells.2007-0484.
55. Darabi, R., Arpke, R.W., Irion, S., Dimos, J.T., Grskovic, M., Kyba, M., Perlingeiro, R.C.R., and Perlingeiro, R.C. (2012). Human ES- and iPS-derived myogenic progenitors restore DYSTROPHIN and improve contractility upon transplantation in dystrophic mice. Cell Stem Cell *10*, 610–619. https://doi.org/10.1016/j.stem.2012.02.015.
56. Barberi, T., Bradbury, M., Dincer, Z., Panagiotakos, G., Socci, N.D., and Studer, L. (2007). Derivation of engraftable skeletal myoblasts from human embryonic stem cells. Nat. Med. *13*, 642–648. https://doi.org/10.1038/nm1533.
57. Laino, G., Graziano, A., d'Aquino, R., Pirozzi, G., Lanza, V., Valiante, S., De Rosa, A., Naro, F., Vivarelli, E., and Papaccio, G. (2006). An approachable human adult stem cell source for hard-tissue engineering. J. Cell. Physiol. *206*, 693–701. https://doi.org/10.1002/jcp.20526.
58. Grabowska, I., Brzoska, E., Gawrysiak, A., Streminska, W., Moraczewski, J., Polanski, Z., Hoser, G., Kawiak, J., Machaj, E.K., Pojda, Z., and Ciemerych, M.A. (2012). Restricted myogenic potential of mesenchymal stromal cells isolated from umbilical cord. Cell Transplant. *21*, 1711–1726. https://doi.org/10.3727/096368912x640493.
59. Zhang, Y., Zhong, J., Lin, S., Hu, M., Liu, J., Kang, J., Qi, Y., Basabrain, M.S., Zou, T., and Zhang, C. (2023). Direct contact with endothelial cells drives dental pulp stem cells toward smooth muscle cells differentiation via TGF-β1 secretion. Int. Endod. J. *56*, 1092–1107. https://doi.org/10.1111/iej.13943.
60. Milner, D.J., Bionaz, M., Monaco, E., Cameron, J.A., and Wheeler, M.B. (2018). Myogenic potential of mesenchymal stem cells isolated from porcine adipose tissue. Cell Tissue Res. *372*, 507–522. https://doi.org/10.1007/s00441-017-2764-z.
61. Lee, J.H., and Kemp, D.M. (2006). Human adipose-derived stem cells display myogenic potential and perturbed function in hypoxic conditions. Biochem. Biophys. Res. Commun. *341*, 882–888. https://doi.org/10.1016/j.bbrc.2006.01.038.

## STAR★METHODS

### KEY RESOURCES TABLE

| REAGENT or RESOURCE | SOURCE | IDENTIFIER |
|---|---|---|
| Antibodies | | |
| Anti-Pax7 | DSHB | Cat#PAX7; RRID: AB_2299243 |
| Anti-Pax7 | Santa Cruz Biotechnology | Cat#sc-81648; RRID: AB_2159836 |
| Anti-MyoD1 | Proteintch | Cat#18943-1-AP; RRID: AB_10603467 |
| Anti-Ki67 | Thermo Fisher Scientific | Cat#14-5698-37; RRID: AB_2865119 |
| Anti-Laminin | Abcam | Cat#ab11575; RRID: AB_298179 |
| Anti-Laminin | Santa Cruz Biotechnology | Cat#sc59854; RRID: AB_784266 |
| Anti-MyHC-IIA | DSHB | Cat#SC-71; RRID: AB_2147165 |
| Anti-MyHC-IIB | DSHB | Cat#BF-F3; RRID: AB_2266724 |
| Anti-MyHC-IIX | DSHB | Cat#MF-20; RRID: AB_2147781 |
| Anti-MyHC-I | DSHB | Cat#BA-F8; RRID: AB_10572253 |
| Anti-human Nucleoli (hNu) | Abcam | Cat#ab190710; RRID: AB_2937055 |
| Anti-SDHA | Proteintch | Cat#14865-1-AP; RRID: AB_11182164 |
| Anti-STEM121 | Cellartis | Cat#Y40410; RRID: AB_2801314 |
| Anti-CD8 | Abclonal | Cat#A23081; RRID: AB_3662930 |
| Anti-CD4 | Abclonal | Cat#A26036; RRID: AB_3662931 |
| Anti-FasL | Santa Cruz Biotechnology | Cat#sc-19681; RRID: AB_626940 |
| Anti-PDL1 | Proteintch | Cat#66248-1-Ig; RRID: AB_2756526 |
| Anti-Desmin | Proteintch | Cat#16520-1-AP; RRID: AB_2292918 |
| Anti-β-actin | Absin Bioscience | Cat#abs830031; RRID: AB_2892540 |
| Alexa Fluor® 488 AffiniPure Donkey Anti-Mouse IgG | Jackson | Cat#715-545-150; RRID: AB_2340846 |
| Alexa Fluor® 488 AffiniPure Donkey Anti-Rabbit IgG | Jackson | Cat#711-545-152; RRID: AB_2313584 |
| Alexa Fluor® 594 AffiniPure Donkey Anti-Mouse IgG | Jackson | Cat#715-585-150; RRID: AB_2340854 |
| Alexa Fluor® 594 AffiniPure Donkey Anti-Rabbit IgG | Jackson | Cat#711-585-152; RRID: AB_2340621 |
| Alexa Fluor® 647 Donkey anti-Rat IgG | Thermo Fisher Scientific | Cat#A78947; RRID: AB_2910635 |
| Anti-rabbit IgG, HRP-linked Antibody | Cell Signaling Technology | Cat#7074; RRID: AB_2099233 |
| Anti-mouse IgG, HRP-linked Antibody | Cell Signaling Technology | Cat#7076; RRID: AB_330924 |
| Critical commercial assays | | |
| H&E staining kit | BOSTER | AR1180 |
| Masson staining kit | Biossci | BP028 |
| DAB Substrate Kit | Solarbio | DA1010 |
| FastQuant RT Kit | TIANGEN | KR116-02 |
| SuperReal PreMix PCR Kit | TIANGEN | FP205-02 |
| Mouse TNF-alpha Uncoated ELISA Kit | ThermoFisher | 88-7324-88 |
| Mouse CRP ELISA Kit | Servicebio | GEM0007 |
| Chemicals, peptides and recombinant proteins | | |
| Minimum Essential Medium α (α-MEM) | Gibco | 12571–063 |
| Dulbecco's Modified Eagle Medium (DMEM) | Gibco | 11965–092 |
| Iscove's Modified Dulbecco's Medium (IMDM) | Gibco | 12440053 |
| Dimethyl sulfoxide (DMSO) | Sigma | D4540 |
| Phosphate-Buffered Saline (PBS) | Hyclone | SH30256.01 |

(*Continued on next page*)

*Continued*

| REAGENT or RESOURCE | SOURCE | IDENTIFIER |
|---|---|---|
| Penicillin-Streptomycin (PS) | Gibco | 15140163 |
| Fetal Bovine Serum (FBS) | Gibco | 16140071 |
| Horse Serum (HS) | Hyclone | SH30074.02 |
| 0.05% Trypsin | Gibco | 25300 |
| 5-Azacytidine (5-Aza) | Sigma | 855049 |
| Noggin | Sino Biological | 10267-HNAH |
| Trizol | Thermo Fisher | 15596018 |
| Triton X-100 | Sigma | SLBT3016 |
| Bovine Serum Albumin (BSA) | Solarbio | 9048-46-8 |
| RIPA lysis buffer | Thermo Fisher | 89900 |
| protease/phosphatase inhibitor cocktail | CST | 5872 |
| DAPI | Abcam | ab228549 |
| BD Vacutainer® SST™ Tubes | BD Vacutainer | 367957 |
| alanine aminotransferase (ALT) | Changchun Huili | C052-day |
| aspartate aminotransferase (AST) | Changchun Huili | C072-e |
| creatinine (Cre) | Changchun Huili | C074-e |
| creatine kinase (CK) | Changchun Huili | C059-b |
| lactate dehydrogenase (LDH) | Changchun Huili | C018-b |
| Experimental models: Cell lines | | |
| C2C12 | Cell Bank/Stem Cell Bank, Chinese Academy of Sciences | CSTR:19375.09.3101MOUSCSP505 |
| Experimental models: Organisms and strains | | |
| SPF mice | SHANGHAI SLAC LABORATORY ANIMAL | C57BL/6J |
| Software and algorithms | | |
| GraphPad Prism | https://www.graphpad.com | |
| LabChart | https://www.adinstruments.com | – |
| ImageJ | https://imagej.nih.gov/ij/ | |

## EXPERIMENTAL MODEL AND STUDY PARTICPANT DETAILS

### DPSC culture

The research proposal for use of human samples were approved by Medical Ethical Committee of Shanghai Stomatological Hospital, Fudan University (No. 2017-0004 and No. 2019-003). We have also obtained informed consents to participate from the human donors. The human donors were Chinese from both genders ranged from 18 to 25 years old. Human third molar (free of caries and/or periodontitis) needed be removed for dental preventive care were collected. It was ensured that the donors' tooth extraction wounds healed well and their pain was minimized. The dental pulp was immediately separated from the teeth, and was cut into 1 $mm^3$ pieces, adhered to a 10 mm dish with α-MEM (Gibco, NY, USA) supplemented with 10% fetal bovine serum (FBS, Gibco, NY, USA) and 1% penicillin–streptomycin (Gibco, NY, USA) at 37°C in the presence of 5% $CO_2$. The medium was changed every 3 days. DPSCs were then cryopreserved in 90% FBS with 10% DMSO in P1, and were expanded to P3 - P4 for further experiments. In this study, we independently included DPSC cultures from twelve donors (8 female, 4 male). DPSCs from each donor were cultured separately, with cell migration not affected by gender. Twelve independent DPSC primary cell cultures were allocated to cell proliferation and myogenic inducing pre-experiments ($n$ = 3), direct coculture system ($n$ = 3), conditional medium preparation ($n$ = 3), and stem cell transplantations ($n$ = 3).

### DSPC myogenic induction

When the confluence reached 80%, DPSCs were induced to a myogenic fate (iDPSCs) with 1 μM 5-aza (Sigma–Aldrich, CA, USA) for 1 day, and followed by 200 ng/mL BMP antagonist Noggin for 7 days. The differentiation medium was changed every 3 days. The myogenic markers were tested by immunofluorescence and western blot analysis. DPSCs and iDPSCs used in each independent experiment were sourced from the same donor.

### Cell hypoxia model

Cells were placed in an incubator controlled by a computerized delivery profile system (OxyCycler C42, Biospherix, Redfield, NY) at 37°C, and connected to $N_2$, $O_2$, and $CO_2$. Set the oxygen concentration to 1% and $CO_2$ to 5%, and adjust the control mode to automatic mode. The intake volume can be automatically adjusted according to the set values. Pre place the culture medium in this hypoxia incubator to reduce the oxygen content in the medium.

### Direct coculture system

The murine myoblast cell line C2C12 was purchased from the Cell Bank/Stem Cell Bank of the Chinese Academy of Sciences and authenticated by the China Center for Type Culture Collection (CSTR:19375.09.3101MOUSCSP505) using Short Tandem Repeat (STR) analysis technology. It was tested not having mycoplasma contamination. C2C12 was cultured in DMEM high glucose with 10% FBS and 1% penicillin-streptomycin at 37°C in 5% $CO_2$. DPSCs were myogenically induced with 5-Aza and the BMP antagonist Noggin (iDPSCs). Then, DPSCs/iDPSCs and C2C12 cells were seeded on 6-well plates (or 24-well plates) at a ratio of 5:1 under 1% $O_2$ hypoxia and maintained in growth medium until the cells reached confluency. At this point, the growth medium was replaced with differentiation medium containing DMEM high glucose plus 2% Horse Serum (HS) and 1% penicillin-streptomycin and continued to be cocultured for 7 days.

### Conditional medium (CM) of DPSCs/iDPSCs

DPSCs/iDPSCs were seeded in 100-mm dishes and, when reaching 70–80% confluence, the mediums were replaced by serum-free DMEM. After 48 h, the supernatant was collected and filtered through a 0.22-μm filter; subsequently, the CM was concentrated 30-fold using an ultrafiltration unit with a 10-kDa molecular weight cutoff (UFC901096, Millipore) centrifuged at 4,000 × g for 25 min at 4°C. Serum-free DMEM without cells was used as control CM, and it was incubated, collected and stored in a similar manner. Then C2C12 myoblasts were treated for 7 days as follows: normoxia + control CM, hypoxia + control CM, hypoxia + CM-DPSCs, and hypoxia + CM-iDPSCs.

### CIH animal model and GG transplantation

Eight-week-old C57BL/6J male mice (Shanghai SLAC Laboratory Animal Co., Ltd) were housed in the animal facility under stable conditions of humidity and temperature on a 12:12 h light-dark cycle with free access to food and water. Male mice are chosen for OSA modeling to exclude estrogen influence. The animal experiments were conducted at Shanghai Model Organisms Center (with License for the Use of Laboratory Animals) in accordance with *Guide for the Care and Use of Laboratory Animals, 8th edition*, and approved by the Institutional Animal Care and Use Committee at the Shanghai Research Center for Model Organisms (SRCMO-IACUC No. 2019–0020–1). Animals were exposed to CIH in chambers controlled by a computerized delivery profile system (Oxycycler Model A84XOV; Biospherix, Redfield, NY) connected to $N_2$ and $O_2$ (Figure 1C). $O_2$ levels ranging from 21% to 7.5% circulated for 180 s, of which 7.5% $O_2$ was maintained for 20 s (Figure 1D). CIH circulation lasted for 8 h per day from 10:00 a.m. to 18:00 p.m. Observe the mice for any abnormal behaviors in excitement, feeding, or overall mental state.

Experimental animals were divided into four groups: normoxia (NOR) ($n = 18$), CIH ($n = 18$), CIH + DPSCs ($n = 18$), and CIH + iDPSCs ($n = 18$) (Figure 1G). Among them, the latter three groups were exposed to CIH circulation. The NOR group was given normal air. DSPCs/iDPSCs from the same source among 3 independent donors were used for each 6 animal repeats. At the end of the 4th week, DPSCs or iDPSCs were injected into the GG using an insulin needle (29 G) (Figure 1E) in CIH + DPSCs and CIH + iDPSCs groups, while the remaining two groups received the same volume of saline. The procedure of GG injection operation: 1) Mice were anesthetized by intraperitoneal injection of 1% pentobarbital (0.1 mL/10 g body weight), and placed in the supine position. 2) Place the mouse in the supine position on the operating platform, and disinfect the mouth with iodophor. 3) Inject at the sublingual side near the root of lingual frenum with insulin needle (29 G) and penetrate parallel to the epidermis of the tissue for about 5 mm. Stem cells solution were injected about 10 μL (10000 cells dissolved in sterilized saline). Monitor the healing of injection wounds in mice to prevent suffocation due to bleeding or edema. During the experiment, the body weight and food and water intake of all mice were measured. After 6 weeks, all mice were sacrificed.

## METHOD DETAILS

### Electromyography of the genioglossus muscle ($EMG^{GG}$)

Mice were anesthetized by intraperitoneal injection of 1% pentobarbital (0.1 mL/10 g body weight) and placed in the supine position. After stripping the neck skin and cervical membrane, the digastric muscles (DM) were exposed. The DM were then separated and removed to expose the GG. Then, the EMG signals of both DM and GG were detected. Two Teflon-insulated wire loop electrodes were used to record electromyographic activity with third electrodes inserted into the tails of mice (Figure 2A). The EMG signals were connected to the Biological Functional System and amplified by bandpass filtering from 1 to 1000 Hz (AD Instrument Australia). LabChart 8 software was used to analyze the experimental results. Eleven channels were set for data acquisition and analysis (Table S1). Because EMG testing could damage tissue structure and result in unstable results, and these GG samples were not used for histological measures or blood collection.

### Serum biochemical index detection

Blood was collected from mouse eyeballs into a blood collection tube (BD Vacutainer) in mice without EMG testing from each group. Then, the mice were sacrificed by cervical dislocation. The blood collection tubes were gently inverted 180° 5–6 times. The serum specimens were

centrifuged at 4000 rpm for 10 min at room temperature and stored at −80°C. Serum enzyme kits were used to mix with these serum specimens by adding a specific amount of reagent R1 or R2 according to the manufacturer's instructions. The R1 and R2 components can be found in Table S2. Subsequently, the serum levels of alanine aminotransferase (ALT), aspartate aminotransferase (AST), creatinine (Cre), lactate dehydrogenase (LDH) and creatine kinase (CK) were measured using the automatic biochemistry analyzer Chemray-800 (Rayto Life and Analytical Sciences). The parameters, such as sample dosage, R1 or R2 reagent dosage, delay time, detection time, detection wavelength, etc., were listed in Table S3.

### ELISA experiments

ELISA experiments were performed following the instructions of the ELISA kit, such as Mouse TNF-alpha Uncoated ELISA Kit (No. 88-7324-88, ThermoFisher), and Mouse CRP ELISA Kit (No. GEM0007, Servicebio). ELISA plate with 100 μL/well of capture antibody in PBS. Seal the plate and incubate overnight at 4°C. Block wells with 200 μL of Diluent Concentrate. Incubate at room temperature for 1 h. Aspirate and wash for a total of 3–5 times. Add 100 μL/well of samples to the appropriate wells. Seal the plate and incubate at room temperature for 2 h. Repeat for a total of 3–5 washes. Add 100 μL/well diluted Detection Antibody to all wells. Seal the plate and incubate at room temperature for 1 h. Repeat for a total of 3–5 washes. Add 100 μL/well of diluted Streptavidin-HRP. Seal the plate and incubate at room temperature for 30 min. Add 100 μL/well of Tetramethylbenzidine Substrate Solution. Incubate at room temperature for 15 min. Add 100 μL/well of Stop Solution. Read plate at 450 nm. Calculate the sample concentration based on the standard curve equation.

### Hematoxylin and eosin staining

The muscles were excised from mice and fixed in ice-cold 4% PFA for further histological measures. Briefly, after deparaffinization and rehydration, 5 μm-thick sections were stained with hematoxylin solution for 3 min followed by 5 s of 1% acid ethanol (1% HCl in 70% ethanol) and then rinsed in running water. Then, the sections were stained with eosin solution for 3 min, followed by running water for 5 min. Dehydration with graded alcohol was then performed. After Histoclear washing, the slides were sealed with neutral gum.

### Masson staining

Soak the dehydrated slices in Bouin's solution and rinse with running water. Next, the sections were stained with iron hematoxylin for 5–10 min, followed by 1% hydrochloric acid alcohol, lithium carbonate for a few seconds, bright spring red for 5-1 min, and phosphomolybdic acid for 5 min. The sections were then stained with aniline blue for 5 min without washing, and then 1% acetic acid for 1 min, and finally seal with neutral gum after dehydration.

### Immunofluorescence

Muscle sections and cultured cells were fixed in 4% paraformaldehyde and permeabilized for 15 min in 0.25% Triton X-100 in PBS. The samples were blocked in 5% BSA for 30 min at room temperature. The samples were then incubated with primary antibodies in 2.5% BSA at 4°C overnight. Subsequently, the samples were washed with 0.5% Tween 20 in PBS (PBST) and stained with anti-mouse Alexa 594 or Alexa 488, anti-rabbit Alexa 594 or Alexa 488 (Jackson ImmunoResearch, PA, USA), anti-rat Alexa 647 for 30 min at room temperature. After washing with PBST, DAPI was used to stain nuclei for 5 min. The primary antibodies used were as follows: antibodies against MyHC-IIA (SC-71, DSHB), MyHC-IIB (BF-F3, DSHB), MyHC-IIX (MF-20S, DSHB), Anti-MyHC-I (BA-F8, DSHB), Pax7 (PAX7, DSHB), Pax7 (sc-81648, Santa Cruz), Ki67 (14-5698-37, Invitrogen), MyoD1 (18943-1-AP, Proteintch), human Nucleoli (ab190710, Abcam), CD8 (A23081, Abclonal), CD4 (A26036, Abclonal), FasL (sc-19681, Santa Cruz), PDL1 (66248-1-Ig, Proteintch), Desmin (16520-1-AP, Proteintch), Laminin (ab11575, Abcam), and Laminin (sc59854, Santa Cruz).

### Immunohistochemistry staining

After deparaffinized and rehydration, the sections were conducted using citric acid buffer, and then 0.05% Triton X-100. Endogenous peroxidase activity was quenched with 3% $H_2O_2$. The sections were blocked with 5% goat serum to prevent non-specific binding and incubated with primary antibodies at 4°C overnight. The primary antibodies used were as follows: antibodies against STEM121 (Y40410, Cellartis) and SDHA (14865-1-AP, Proteintch). The following day, sections were washed with PBST and incubated with horseradish peroxidase (HRP)-conjugated secondary antibodies for 1 h at room temperature. After additional washes, chromogenic detection was performed using the DAB Substrate Kit (DA1010, Solarbio). Sections were counterstained with hematoxylin, sequentially dehydrated with ethanol and xylene, and mounted.

### RNA extraction and reverse transcription-quantitative polymerase chain reaction (RT-qPCR)

Total RNA was extracted from coculture cells and genioglossus tissue using TRIzol reagent (Invitrogen, Carlsbad, CA, USA). cDNA was synthesized using a FastQuant RT Kit (Tiangen, Beijing, China). SuperReal PreMix (Tiangen Biotech Co., Ltd.) was used for amplification of cDNA to the relative mRNA of genes on a Light Cycler 96 system (Roche, Basel, Switzerland) using a Real-Time PCR System (Biometra Biomedizinische Analytik GmbH). The primer sequences utilized for RT−qPCR can be found (Table S4). Relative mRNA expression was calculated using the $2^{\Delta\Delta Cq}$ method.

### Western blot analysis

The whole cell lysate was prepared with RIPA lysis buffer (89900, Thermo Fisher, MA, USA) plus protease/phosphatase inhibitor cocktail (5872, CST, MA, USA) at 25 mg protein lysate. SDS PAGE was performed on Mini-PROTEAN Tetra Precast Gels (Bio-Rad) and transferred using Mini Trans-Blot Cell (Bio-Rad) by PowerPac Basic Power Supply (Bio-Rad). Pax7 (PAX7, DSHB), MyoD1 (18943-1-AP, Proteintch) and β-actin (abs830031, Absin Bioscience) were blotted as a primary antibody for overnight. Secondary antibodies, anti-rabbit IgG (7074S, CST) and anti-mouse IgG (7076S, CST) were blotted afterward. The membranes were visualized using Super Signal West Dura substrate (Thermo Scientific, MA, USA), and the bands were detected with an AI600 imager (GE Healthcare, IL, USA).

## QUANTIFICATION AND STATISTICAL ANALYSIS

The experimental data are expressed as the mean ± standard error (mean ± SEM), and the data were analyzed and plotted by GraphPad Prism 5 software. For comparison of two samples, Student's *t* test was used. For comparison of multiple groups of samples, ANOVA was used, followed by Fisher's LSD test for multiple comparison. $*p < 0.05$, $**p < 0.01$, and $***p < 0.001$ represent statistically significant differences, and NS represents no statistically significant differences.